# Alumina-embedded HZSM-5 with enhanced behavior for the catalytic cracking of biomass pyrolysis bio-oil: Insights into the role of mesoporous matrix in the deactivation by coke

Iratxe Crespo, Jasmine Hertzog, Vincent Carré, Frederic Aubriet, Beatriz Valle

Journal of Analytical and Applied Pyrolysis 172 (2023) 106009

Contents lists available at ScienceDirect

Journal of Analytical and Applied Pyrolysis

journal homepage: www.elsevier.com/locate/jaap

# Alumina-embedded HZSM-5 with enhanced behavior for the catalytic cracking of biomass pyrolysis bio-oil: Insights into the role of mesoporous matrix in the deactivation by coke

Iratxe Crespo [a], Jasmine Hertzog [b], Vincent Carré [b], Frédéric Aubriet [b], Beatriz Valle [a,*]

[a] Department of Chemical Engineering, University of the Basque Country (UPV/EHU), P.O. Box 644, Bilbao 48080, Spain
[b] Université de Lorraine, LCP-A2MC, 57078 Metz, France

ARTICLE INFO

*Keywords:*
Bio-oil
Cracking
HZSM-5
$Al_2O_3$ matrix
Coke deactivation
BTEX

ABSTRACT

The behavior of HZSM-5 zeolite embedded in γ-$Al_2O_3$/α-$Al_2O_3$ matrix in the catalytic cracking of biomass pyrolysis bio-oil was studied with special focus on the role of the matrix in the deactivation by coke. The runs were conducted at 450 ºC, space-time of 0.35 $g_{zeolite}.h.g_{feed}^{-1}$ and 0.5 h, 1 h, and 2 h on stream. The analysis of reaction products was conducted by in-line GC and GC/MS, and deactivated catalyst samples were extensively characterized by $N_2$ physisorption, $NH_3$-TPD, TPD-TPO, TPD-GC/MS and LDI FT-ICR MS. The alumina-embedded catalyst (Cat−Z30) exhibited greater stability, keeping the bio-oil conversion above 88 % for 0.5 h on stream, in comparison to the bulk HZSM-5 that deactivated rapidly entailing a bio-oil conversion plunge (from 95 % to 40 %). Consequently, the yield of gasoline-range hydrocarbons (> 70 % MAH monoaromatics) was boosted from 18 % to 26 % for the same reaction time. The aqueous liquid byproduct concurrently produced has a suitable composition for $H_2$ production by further steam reforming. The enhanced behavior was caused by the weak-acid mesoporous structure of the matrix playing a dual function: i) *diffusive-shell* (inwards) role by promoting fragmentation/deoxygenation of bulky molecules (e.g., saccharides and guaiacols) into reactive oxygenates, and deposition of thermally-induced coke away from the zeolite micropores; ii) *spread-growth* (outwards) role by enhancing the diffusion of hydrocarbons outwards from zeolite crystals, and by promoting the development of heavy polycyclic structures that delay the blockage of active sites in micropores. The results are useful to progress towards the integral valorization of raw bio-oil, the development of active and stable catalysts, and the proposal of regeneration strategies necessary for the scaling up.

## 1. Introduction

The potential of sustainable biomass-based industry has an increasingly recognition for partially replacing of fossil resources and reducing the net greenhouse gas (GHG) emissions. However, biomass conversion still needs to face significant challenges to compete with petroleum technologies for the production of bio-fuels and chemicals. In this scenario, the conversion of biomass-derived liquid (bio-oil) arises at the heart of most bio-refinery design proposals [1].

Fast pyrolysis of lignocellulosic biomass is widely regarded as a promising and cost-effective technique for producing bio-oil using relatively simple technology with low environmental impact [2,3]. The raw bio-oil produced is composed of a wide range of oxygenates (saccharides, carboxylic acids, phenols, esters, furans, etc.) which makes it a potentially rich source of value-added products such as hydrogen, bio-fuels, and platform chemicals [4]. The research on bio-oil valorization has been focused on the development of ad hoc designed catalytic processes, with the production of $H_2$ by steam reforming and hydrocarbon fuels and chemicals by cracking and hydroprocessing being the main alternatives. One of the well-known challenges for the successful scaling up is the great catalyst deactivation by coke deposition. Therefore, advancement in catalyst deactivation mitigation plays an instrumental role for boosting the competitiveness of biomass conversion technologies [5]. Co-processing of bio-oil with petroleum feedstock has also attracted great attention with the aim of integrating well-established refinery technologies in the development of biorefinery [6–8].

The catalytic cracking arises as a versatile alternative that can create

* Corresponding author.
*E-mail address:* beatriz.valle@ehu.es (B. Valle).

https://doi.org/10.1016/j.jaap.2023.106009
Received 21 February 2023; Received in revised form 26 April 2023; Accepted 12 May 2023
Available online 16 May 2023

attractive opportunities for the valorization of bio-oil, targeted to the production of bio-fuels and/or platform chemicals according to market demand. The operating conditions at atmospheric pressure and without $H_2$ supply would be a major advantage in terms of cost competitiveness and feasibility over hydrotreating [9]. Conversion of bio-oil oxygenates over acid catalysts entails numerous reaction pathways, involving deoxygenation (decarboxylation, decarbonylation, dehydration), cleavage of C–C bonds, oligomerization/cracking, alkylation, and hydrogen-transfer reactions. Zeolite based catalysts have been generally used in the studies on bio-oil cracking [4,10], in which zeolites with MFI morphology (e.g., ZSM-5) have revealed great selectivity to BTEX (benzene, toluene, ethylbenzene and xylenes) [11,12]. These aromatic hydrocarbons are basic chemicals of increasing demand for the production of plastics, fibers, pesticides and fuel blending additives. In a recent comparison with HY zeolite (FAU morphology), the capability of ZSM-5 zeolite for BTEX production was attributed to its greater activity for oligomerization-cyclization-condensation of light olefins formed as primary products by dehydration/cracking of the oxygenates contained in real bio-oil feed [13]. The hydrogenolysis of catechols derived from phenolic ethers in the bio-oil may also contribute to aromatics formation.

The main challenge to be faced by the conversion of pyrolysis bio-oil with microporous HZSM-5 is the design of catalyst particles that enhance the access of bulky bio-oil molecules to the active acid sites while minimizing the deactivation by coke deposition [14,15]. Among the strategies, the most widely reported has been the development of intrinsic hierarchical porous structure [16–18]. However, the successful scaling up of the process requires a feasible adaption of laboratory protocols for optimal catalyst preparation for multi-ton manufacture. In technical/industrial catalysts manufacturing, it is common to include additives along with the active phase for improving physical, chemical and mechanical properties, which may have a great impact on the catalytic performance. Mitchell et al. [19] emphasized the need to apply available techniques for in-depth assessing of physicochemical properties and catalyst behavior in order to establish synthesis–property–function relationships for these industrial-adapted catalysts. In the case of poor self-binding zeolites, the use of binders is essential to attain particles with the required mechanical strength when using reactors with fluidized bed configurations. Paradigmatic is the use of mesoporous matrixes for improving the diffusion of bulky hydrocarbon molecules to Y zeolite active sites in commercial FCC (fluidized catalytic cracking) catalysts [20,21]. The agglomeration of HZSM-5 zeolite within an alumina matrix has been previously addressed in light oxygenates conversion, such as MTO (methanol-to-olefins) [22] and DTO (dimethyl ether-to-olefins) [23]. The increased catalyst lifetime was attributed to the diffusion of coke precursors outwards zeolite crystals, thus avoiding their confinement and evolution over the acid sites [24].

In this work, we investigate the effect that the mesoporous $\gamma$-$Al_2O_3$/$\alpha$-$Al_2O_3$ matrix has in the behavior of HZSM-5 catalyst during the catalytic cracking of real raw bio-oil produced by biomass pyrolysis. Special attention has been paid on the role of the matrix on the coke deposition by using different techniques to analyze the deterioration of catalyst properties and the nature and location of coke. In addition to conventional techniques, such as $N_2$ physisorption, temperature-programmed desorption of ammonia ($NH_3$-TPD), and temperature-programmed desorption/oxidation (TPD-TPO), we propose innovative approaches for the characterization of coke species at the molecular-level. Temperature-programmed desorption of deactivated catalyst samples was conducted in-line with gas chromatography/mass spectrometry (TPD-GC/MS) to elucidate inert-flow removable species, as a novel and low time-consuming technique alternative to extraction-analysis of soluble coke. Fourier-transform ion cyclotron resonance mass spectrometry (FT-ICR MS) is a novel high-resolution technique that has been used to analyze the molecular composition and structure of a wide variety of complex solid and liquid samples [25–27]. Recent studies have shown its applicability to study the coke deposited during the conversion of simple organic molecules (e.g., methanol, ethylene) [28,29]. However, precise analyses of the coke species formed in the conversion of complex feedstock are still scarce. Previous studies by Aubriet et al. [30,31] are pioneering works on the combination of laser desorption ionization (LDI) with FT-ICR MS for the molecular-level elucidation of heavy species contained in biomass derived bio-oil and bio-char. In this work, we applied the LDI FT-ICR MS technique to provide a comprehensive molecular fingerprint of the coke deposited in the matrix and HZSM-5 zeolite crystals during the cracking of raw bio-oil.

The combination of results provides insights into the content, composition and prevailing location of coke, thus helping to understand the formation and growth of deactivating coke species on HZSM-5 catalyst, which is an essential information to address the scaling up of the process with optimal regeneration strategy [32]. The findings of this paper would well contribute to the development of biorefineries focused on biomass waste pyrolysis processes.

## 2. Materials and methods

### 2.1. Preparation of catalysts

A commercial ZSM-5 zeolite with $SiO_2/Al_2O_3$ = 30 (*CBV-3024E* provided by *Zeolyst International* in ammonium form) was used in two different configurations: bulk HZSM-5 catalyst (named Zeo−Z30) and alumina-embedded HZSM-5 catalyst (named Cat−Z30).

The Zeo−Z30 catalyst was prepared by calcination of as-received zeolite in a furnace at 5 °C.min$^{-1}$ up to 575 °C for 2 h, with the aim of converting $NH_4$-ZSM-5 zeolite into active H-ZSM-5 form suitable as a catalyst. The calcined powder was then subjected to compression using a *Herzog TP40* Manual Press (keeping a 600 kN pressure for 15 min). The resulting pellets were then crushed and sieved into particles of 150–300 μm.

The agglomeration method by wet extrusion was followed to prepare the alumina-embedded HZSM-5 catalyst. Firstly, high-purity dispersible pseudo-boehmite (DISPERAL 70 % $Al_2O_3$ *Sasol*) was added to a colloidal dispersion of $\alpha$-$Al_2O_3$ (20 % in water, *Alfa Aesar*) and homogeneously mixed by continuous stirring. Then, the zeolite powder was slowly added in the accurate amount to obtain a catalyst with 50 wt. % of zeolite, 30 wt. % pseudo-boehmite, and 20 wt. % $\alpha$-$Al_2O_3$. The stirring was kept for 3 h until a uniform slurry was obtained, which was then extruded and dried overnight at room temperature. Afterwards, the dried extrudates were crushed and sieved into 150–300 μm particles. The final catalyst was obtained after calcination at 5 ºC.min$^{-1}$ up to 575 °C for 2 h. Through the calcination, pseudo-boehmite was converted into $\gamma$-$Al_2O_3$, which is its stable phase at this temperature.

### 2.2. Characterization of catalysts

#### 2.2.1. Physico-chemical properties of fresh and deactivated catalysts

The textural properties of fresh Zeo−Z30 and Cat−Z30 catalysts (Table 1) were determined by $N_2$ physisorption using a *Micromeritics ASAP 2010* device. The Brunauer-Emmet-Teller (BET) equation was used to quantify the specific surface area. The external surface area ($S_{Ext}$) and micropore volume ($V_{Micro}$) were calculated using the *t*-plot method. The total pore volume was based on the volume adsorbed at $P/P_0$ = 0.995 and the mesopore volume ($V_{Meso}$) was calculated by difference.

**Table 1**
Physico-chemical properties of fresh Zeo−Z30 and Cat−Z30 catalysts.

| | Zeo−Z30 | Cat−Z30 |
|---|---|---|
| $S_{BET}$ ($m^2.g^{-1}$) | 428 | 267 |
| $S_{Ext}$ ($m^2.g^{-1}$) | 31 | 138 |
| $V_{Meso}$ ($cm^3.g^{-1}$) | 0.07 | 0.31 |
| $V_{Micro}$ ($cm^3.g^{-1}$) | 0.17 | 0.06 |
| Acidity ($\mu mol_{NH3}.g^{-1}$) | 649 | 354 |

The textural properties of deactivated samples of catalysts were also determined by $N_2$ physisorption.

The acidity (total amount of acid sites) of fresh and deactivated catalyst samples were analysed by temperature-programmed desorption of $NH_3$ ($NH_3$-TPD) using a *Micromeritics AutoChem II 2920* device equipped with a Thermal Conductivity Detector (TCD) calibrated for $NH_3$. Each sample was outgassed in a He flow for 1 h at 550 °C (15 °C.min$^{-1}$) and then cooled down to 150 °C. Afterwards, the sample was saturated with $NH_3$ by continuous injection of 150 μL.min$^{-1}$ ($NH_3$ 10 vol. % in He). After removing the physisorbed $NH_3$ (by flushing with 20 mL.min$^{-1}$ He) desorption of quimisorbed $NH_3$ (TPD) was monitored (TCD signal) until 550 °C with a ramp of 5 °C.min$^{-1}$. The same procedure was used to determine the acidity of the alumina matrix by performing the analysis of a solid sample prepared by the agglomeration method without using zeolite (only matrix). The result evidences a weak acidity (0.06 $mmol_{NH3}.g^{-1}$) that can be attributed to Lewis acid sites of γ-$Al_2O_3$ [13].

### 2.2.2. Content and nature of coke

The content and nature of coke deposited on deactivated catalyst samples was assessed by temperature programmed desorption-oxidation (TPD-TPO) analyses, conducted in a *TA Instruments Q5000* thermobalance following a specifically designed procedure. Each sample was firstly subjected to temperature programmed desorption (TPD) under inert atmosphere (50 mL.min$^{-1}$ $N_2$ flow) by heating at 5 ºC.min$^{-1}$ up to 700 ºC and held for 30 min. Then, it was cooled down to 25 ºC and subjected to temperature programmed oxidation (TPO) under oxidizing atmosphere (50 mL.min$^{-1}$ air flow) by heating at 5 ºC.min$^{-1}$ up to 700 ºC. The coke species released during the TPD stage were ascribed to a *soft coke* that is removed without the need of combustion, whereas the species removed during the TPO stage were ascribed to a *hard coke*.

### 2.2.3. Composition of coke

The composition of the coke deposited on each deactivated catalyst sample was analyzed by combining two spectrometry techniques: temperature programmed desorption in-line with gas chromatography/mass spectrometry (TPD-GC/MS), and laser desorption ionization (LDI) combined with Fourier transform ion cyclotron resonance (FT-ICR) mass spectrometry.

The TPD-GC/MS analyses were performed on a *CDS 6150 Pyroprobe* connected in-line to gas chromatograph/mass spectrometer *GC/MS Shimadzu QP2010* provided with BPX5 column (50 m × 0.22 mm × 0.25 μm). These analyses allowed us to identify the coke species released under inert atmosphere (*soft coke*) making a distinction between those removed below 250 ºC, *low temperature−soft coke* (*LT-SC*), and those removed at higher temperature (700 ºC), *high temperature−soft coke* (*HT-SC*). For this purpose, each sample (10 mg) was loaded in a quartz tube and placed into the Pyroprobe heating coil. It was thermally desorbed under inert atmosphere (30 mL min$^{-1}$ He flow) at 250 °C for 1 min, and the released species (*LT-SC*) were analyzed by GC/MS connected in-line through a heated line (320 ºC). Then, the remaining sample was subjected to the same procedure conducted at 700 °C and the released compounds (*HT-SC*) analyzed by in-line GC/MS.

The LDI FT-ICR MS analyses were performed with a 7 T FT-ICR mass spectrometer (*Solarix 2XR Bruker Daltonics*) equipped with LDI source (*Bruker Daltonics*). In this work, both ion source and instrument parameters were optimized via software FTMS-Control V2.3.0 (*Bruker Daltonics*). Mass spectrometer was externally calibrated and ICR detection cell was shimmed and gated using direct introduction of a 0.1 mg.mL$^{-1}$ sodium trifluoroacetate solution in ESI source. The mass spectra were acquired in negative-ion mode over a 107.5 – 1500 *m/z* range with a 4 megaword time-domain, and result from 20 scans acquisition. Solid catalyst samples were deposited on stainless steel target. A 355 nm wavelength laser with a spot diameter of 20 μm and 40 Hz frequency was used and the ions generated over 100 laser shots were stored in a hexapole before to be transferred into the ICR cell. Laser power was optimized to detect MS signals limiting the fragmentation and recombination phenomenon [33]. A very high mass resolution (higher than 370 000 at *m/z* 350) was achieved. *DataAnalysis 5.2* software (Bruker, Daltonics) were used to internally calibrate the FT-ICR mass spectra with a list of known fatty acids and bio-oil compounds with a standard deviation of mass error ≤ 500 ppb. Peak lists at signal-to-noise ratio ≥ 6 of the different mass spectra were exported and aligned into a matrix according to their *m/z* value in a 1 ppm tolerance window. Peak list assignment was performed by *Composer software-Sierra Analytics*. The molecular formulae were assigned within a ± 0.8 ppm mass error range, with the C, H, O, N, S, and Al elements, and both radical cations and deprotonated ions were considered. This resulted into CH, $CHO_x$, $CHS_1O_x$, and $CHAl_1O_x$ molecular series. The compounds were represented into van Krevelen diagram, according to their oxygen-to-carbon (O/C) and hydrogen-to-carbon (H/C) ratios, which allows distinguishing biochemical classes such as lipids and lignin derivatives [34]. The DBE (double bound equivalent) was calculated by Eq. (1), with $n_C$, $n_H$, and $n_N$ being number of carbon, hydrogen, and nitrogen atoms, respectively. The DBE versus carbon number (#C) graph gives information on the aromaticity and unsaturation degree of a molecule.

$$DBE = 1 + n_C - \left(\frac{n_H}{2}\right) + \left(\frac{n_N}{2}\right) \quad (1)$$

## 2.3. Catalytic cracking runs

### 2.3.1. Bio-oil feed

The raw bio-oil, provided by *Biomass Technology Group-BTG* (The Netherlands), was produced by fast pyrolysis of pine sawdust. The as-received bio-oil was mixed with 20 wt. % of methanol (*Sigma-Aldrich*, ≥ 99.8 %), which has been commonly used as a stabilizing agent to minimize the aging effects during long storage periods and transportation. Methanol acts as a stabilizer by reducing the acidity of raw bio-oil and the formation of reactive carbonyl compounds prone to oligomerization through neutralization, esterification, and etherification reactions [35]. The addition of methanol causes changes in raw bio-oil by neutralization, esterification, and etherification reactions that lead to lower contents of reactive carbonyl compounds prone to oligomerization. The resulting bio-oil/methanol mixture (stabilized bio-oil) has a greater $H/C_{eff}$ ratio with positive effects on subsequent catalytic processing in terms of products selectivity and catalyst stability [36,37]. For the scale-up of the process in accordance with the bio-refinery's objectives, it would be appropriate for methanol to be obtained from bio-syngas derived from the gasification of nonedible biomass [38,39].

The stabilized bio-oil used in this work was composed of 18 wt. % water (determined by Karl Fischer titration using *KF Titrino Plus 870*), 16 wt. % methanol and 66 wt. % of bio-oil derived oxygenates. The detailed composition of these oxygenates (shown in Table S1, Supplementary material) was determined by gas chromatography/mass spectrometry of liquid samples conducted on the *GC/MS Shimadzu QP2010* device. The majority compounds identified in the stabilized bio-oil were saccharides (19 wt. %), phenols (17 wt. %), esters (16 wt. %), acids (15 wt. %) and ketones (15 wt. %).

### 2.3.2. Reaction equipment and product analyses

The stabilized bio-oil was fed into the thermal unit of a two-step catalytic cracking system operating at atmospheric pressure (Fig. S1). In this unit, ca. 9 wt. % of bio-oil oxygenates (mainly phenolic compounds derived from the pyrolysis of biomass lignin) polymerized into a carbonaceous solid (pyrolytic lignin), and ca. 8 wt. % decomposed into gases (CO, $CO_2$, and $CH_4$). The exiting volatile stream entered the in-line catalytic cracking unit (fluidized bed reactor) where the catalyst was located. This volatile feed was composed of water (20 wt. %), methanol (18 wt. %), and bio-oil derived oxygenates (62 wt. %). The detailed composition of these oxygenates analyzed by GC/MS is provided in Table S2, where esters (25 wt. %), acids (23 wt. %), ketones (18 wt. %),

saccharides (12 wt. %), and phenols (7 wt. %) were identified as majority compounds. In the valorization of raw bio-oil, the prior separation of pyrolytic lignin by controlled polymerization of phenolic bio-oil oxygenates in the thermal unit is an effective strategy to reduce coke deposition on the catalyst [40]. It is worth noting that this carbonaceous byproduct could be utilized through gasification to produce methanol, which is used for the stabilization of bio-oil. This approach can contribute significantly to the sustainability and economic viability of the process.

All the runs were carried out under the same operating conditions. The temperature on the catalytic unit was 450 ºC and the thermal unit was kept at 500 ºC, which is a suitable temperature for a good compromise between product yields and catalyst stability [41]. Given that the flow-rate of the bio-oil feed was the same (0.1 mL.min$^{-1}$), the experiments with Zeo−Z30 catalyst were conducted with half the mass (1.5 g) of those conducted with Cat−Z30 (3 g) in order to have the same amount of HZSM-5 zeolite (active sites) in the catalytic bed. Each catalyst was mixed with inert solid (CSi, 100 μm) to ensure good fluid dynamic conditions in the catalytic bed (25 g total). As a result, the space-time referred to zeolite was the same in all the runs (0.35 $g_{zeolite}$.h.$g_{feed}^{-1}$).

Three catalytic cracking runs were conducted with each catalyst by varying duration (0.5 h, 1 h and 2 h) in order to collect deactivated samples at different values of time on stream. During each run, a representative small sample of the product stream was sent (every 10 min) through a heat-insulated line to *Agilent 490 micro-GC* device, provided with four analytical modules for the analysis of: 1) $H_2$, $N_2$, $CH_4$, CO (Molecular sieve column MS5A); 2) $C_4$−$C_{12}$ bio-oil oxygenates, $C_{5+}$ hydrocarbons (CPSil 5CB column); 3) $CO_2$, $C_2$−$C_4$ hydrocarbons, $H_2O$, MeOH, dimethyl ether, $C_2$−$C_4$ oxygenates (PPQ column), 4) $C_6$−$C_{12}$ aromatics, $C_6$−$C_{12}$ oxygenates (Stabilwax).

In addition to the on-line analysis of the volatile stream, the detailed composition of condensable compounds was analyzed by gas chromatography/mass spectrometry (*GC/MS Shimadzu QP2010 device*). The product stream was cooled at the reactor outlet (Peltier condenser) and collected in a steel vessel, which was emptied at stablished intervals (0–0.5 h, 0.5–1 h, and 1–2 h). The liquid collected was composed of an aqueous fraction and organic fraction, which were separated and then analyzed by GC/MS.

### 2.3.3. Parameters for quantifying the catalytic behavior

The performance of bulk zeolite (Zeo−Z30 catalyst) and alumina-embedded zeolite (Cat−Z30 catalyst) was evaluated in terms of reactants conversion (bio-oil oxygenates and methanol contained in the feed) and hydrocarbon yields (grouped into gaseous $C_2$−$C_4$ and liquid $C_{5+}$ compounds). The yield of deoxygenation by-products (CO, $CO_2$, and water) were also quantified.

The conversion of bio-oil and methanol contained in the feed was quantified from the mass flow-rate at the inlet and outlet of the catalytic reactor, according to:

$$X_{Bio-oil}(\%) = \frac{F^{in}_{bio-oil} - F^{out}_{bio-oil}}{F^{in}_{bio-oil}} 100 \quad (2)$$

$$X_{MeOH}(\%) = \frac{F^{in}_{MeOH} - F^{out}_{MeOH}}{F^{in}_{MeOH}} 100 \quad (3)$$

The mass flow-rate of bio-oil oxygenates at the reactor outlet ($F^{out}_{bio-oil}$) was calculated from the molar flow-rate, quantified by the in-line GC analyses by applying calibrating factors to chromatographic areas and using $N_2$ as internal standard. Specifically, 68 chromatographic peaks ascribed to oxygenate compounds were detected (50 in CPSil 5CB column, 6 in PPQ column, and 12 in the Stabilwax column). The calibrating factors of certain oxygenates (methanol, acetone, hydroxyacetone, acetic acid, and phenol) were determined by analyzing known-concentration mixtures of these compounds. The peaks ascribed to unknown oxygenates were grouped into different families (in accordance to proximity to known oxygenates) to which a factor was assigned. The calibration factors of these compounds were determined by analyzing different flow-rates of bio-oil/MeOH feed without catalyst ("thermal" runs) by closing overall mass balance and C balance (below 5 % error).

In addition to the overall conversion of bio-oil oxygenates, Eq. (2), the individual conversion of certain oxygenates contained in the bio-oil was quantified with the aim of assessing whether the reactivity of these compounds is affected by the presence of the alumina matrix, Eq. (4). Specifically, the conversion of the majority compounds in each family was tracked, i.e., methyl formate (esters), acetic acid (acids), hydroxyacetone (ketones), levoglucosan (saccharides), and phenolic ethers (phenols).

$$X_i(\%) = \frac{F^{in}_i - F^{out}_i}{F^{in}_i} 100 \quad (4)$$

where $F^{in}_i$ and $F^{out}_i$ are the mass flow-rates of each oxygenate at the reactor inlet and outlet, respectively. These values were quantified from the mass flow-rate of oxygenates at the inlet ($F^{in}_{bio-oil}$) and outlet ($F^{out}_{bio-oil}$) and the content of each compound, determined by GC/MS analysis of the aqueous fraction collected during three time intervals (0–0.5 h, 0.5–1 h, and 1–2 h).

The product yields were quantified from the mass flow-rate of reactants at the reactor inlet ($F^{in}_{bio-oil} + F^{in}_{MeOH}$) and the mass flow-rate of each product at the reactor outlet ($F^{out}_p$, p = $C_2$−$C_4$, $C_{5+}$, CO, $CO_2$, water) quantified by on-line GC analyses, according to Eq. (5). It should be mentioned that the yield of water produced accounts for that formed in the cracking reactions (not considering the water content in the bio-oil).

$$Y_P(\%) = \frac{F^{out}_p}{F^{in}_{bio-oil} + F^{in}_{MeOH}} 100 \quad (5)$$

In order to assess whether the alumina matrix affects the distribution of liquid $C_{5+}$ hydrocarbons, these were grouped according to their aliphatic and aromatic nature into the following lumps: BTEX (benzene, toluene, ethylbenzene, xylenes), gasoline-range $C_5$-$C_{12}$ hydrocarbons (alkylbenzenes, naphthalenes, aliphatics) and $C_{12+}$ polyaromatics (PAHs). The yield of each constituent lump ($Y_i$) was estimated from the total yield of $C_{5+}$ produced ($Y_{C5}$) and the content of each lump, determined by GC-MS analysis of the organic fraction collected during three time intervals (0–0.5 h, 0.5–1 h, and 1–2 h).

## 3. Results and discussion

### 3.1. Role of alumina matrix on HZSM-5 catalytic behavior

Fig. 1 compares the evolution with time on stream (TOS) of the conversion of oxygenates in the bio-oil (Fig. 1a), the conversion of methanol (Fig. 1b) and the hydrocarbons yields (Fig. 1c) and by-products (Fig. 1d) with bulk HZSM-5 zeolite (Zeo−Z30 catalyst) and alumina-embedded zeolite (Cat−Z30 catalyst). In addition to these results, it is worth mentioning that Cat−Z30 was experimentally found to have greater mechanical resistance to attrition in the fluidized bed reactor.

Fig. 1 shows that high initial values (at zero time on stream) of bio-oil conversion (> 95 %), methanol conversion (> 97 %), and hydrocarbon yields (10 % $C_2$-$C_4$ and 26 % $C_{5+}$) are attained with both catalysts. This similarity of results is consistent with the fact that both runs were conducted with the same value of space-time referred to HZSM-5 zeolite (0.35 $g_{zeolite}$ h $g_{feed}^{-1}$) and the low cracking activity of the matrix (consistent with its low acidity). However, the evolution with TOS reveals clear differences attributable to the presence of the matrix. Thus, a rapid loss of activity can be observed for Zeo−Z30 catalyst, with a sharp decrease in bio-oil conversion (from 95 % to 40 %, Fig. 1a) and methanol

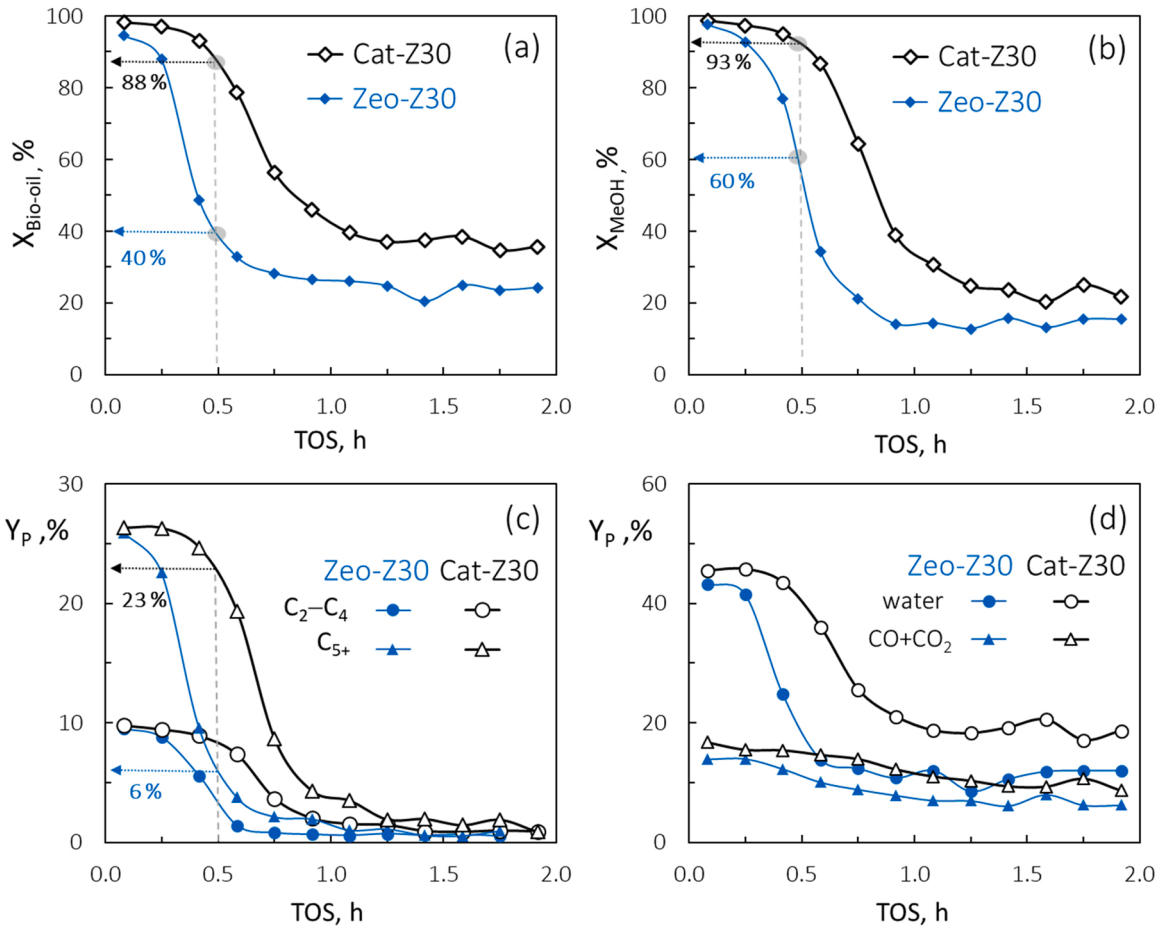


**Fig. 1.** Comparison of the evolution with time on stream of bio-oil conversion (a), methanol conversion (b), yields of hydrocarbon products (c) and by-products (d) using bulk HZSM-5 (Zeo−Z30) and alumina-embedded HZSM-5 (Cat−Z30).

conversion (from 98 % to 60 %, Fig. 1b) in 0.5 h on stream. Accordingly, a sharp decrease in hydrocarbon yields can be noticed (Fig. 1c). In comparison, the Cat−Z30 catalyst undergoes notably slower deactivation, keeping the bio-oil conversion above 88 %, methanol conversion above 93 %, and $C_{5+}$ hydrocarbons yield above 23 % for the same time on stream (Fig. 1c). It should be mentioned that $C_2$-$C_4$ light hydrocarbons are presumably the main products from the conversion of methanol over HZSM-5 under the reaction conditions of this work (450 ºC space-time of (0.35 $g_{zeolite}$ h $g_{feed}^{-1}$) [42].

A noteworthy result is the difference in the pseudo-steady value of oxygenates conversion reached when both catalysts are practically deactivated for hydrocarbon production, which is notably higher with Cat−Z30 catalyst (Fig. 1a). For this catalyst, the yield of deoxygenation byproducts (especially water) is higher (Fig. 1d), and a slightly greater yield of water is observed at the pseudo-steady state. These differences in the yields of byproducts suggest that the presence of the alumina matrix promotes deoxygenation/primary cracking of oxygenates, especially dehydration reactions, so that the Cat-Z30 maintains a remaining activity for these reactions, even when the zeolite is deactivated for the production of hydrocarbons. This matrix activity affects the composition of oxygenates in the liquid product (as will be discussed later).

In addition to the evolution of overall conversion of bio-oil oxygenates (Fig. 1a), the individual conversion of several oxygenates in the bio-oil was quantified according to Eq. (4), and the results are depicted in Fig. 2. These selected oxygenates are the major compounds identified in the feed (Table S2), i.e., acetic acid (22 wt. %), methyl formate (12 wt. %), hydroxyacetone (9 wt. %), levoglucosan (10 wt. %), and phenolic ethers (7 wt. %). In the literature, the catalytic cracking of bio-oil oxygenates has been usually addressed as pure model compounds or composing synthetic mixtures representative of bio-oil [43–46]. The significance of our results lies in the fact that they give information on the reactivity of each compound accounting for the possible synergies with other oxygenates present in the bio-oil. Fig. 2 shows the evolution with time on stream of the individual conversion of selected oxygenates which gives information on the effect that the alumina matrix has on the extent and/or pathways of reactions involving these molecules in a real bio-oil feed.

The results reveal a higher conversion of all oxygenates with Cat−Z30 catalyst (Figs. 2b and 2d) compared with Zeo−Z30 (Figs. 2a and 2c). The enhancement of light oxygenates conversion is evidenced by the higher conversion of acetic acid in the 0–0.5 h range (70 % vs. 92 %). This effect is maintained in the 0.5–1 h interval (43 % vs. 61 %), in which the conversion of hydroxyacetone is boosted even to a greater extent (12 % vs. 49 %). These results evidence that the presence of the mesoporous matrix favors the access of these molecules to the active sites of the zeolite. Regarding the heavier oxygenate compounds, the conversion of levoglucosan ($C_6H_{10}O_5$ formula) and especially the conversion of phenolic ethers ($C_8H_{10}O_2$ as average formula) is clearly promoted with Cat−Z30 (Fig. 2d) in comparison to Zeo−Z30 catalyst (Fig. 2c). This observation suggests that the increased residual activity of Cat-Z30 above 1 h on stream (as shown in Fig. 1a) could be linked to the conversion of these compounds, which undergo deoxygenation/primary cracking (especially dehydration reactions) due to the presence of the alumina matrix.

In addition to the higher activity of Cat−Z30 for the conversion of phenolic ethers (Fig. 2c), some compositional differences were detected among the phenolic compounds collected in the 0–0.5 h range, which suggest that the alumina matrix also affects the reaction pathways of

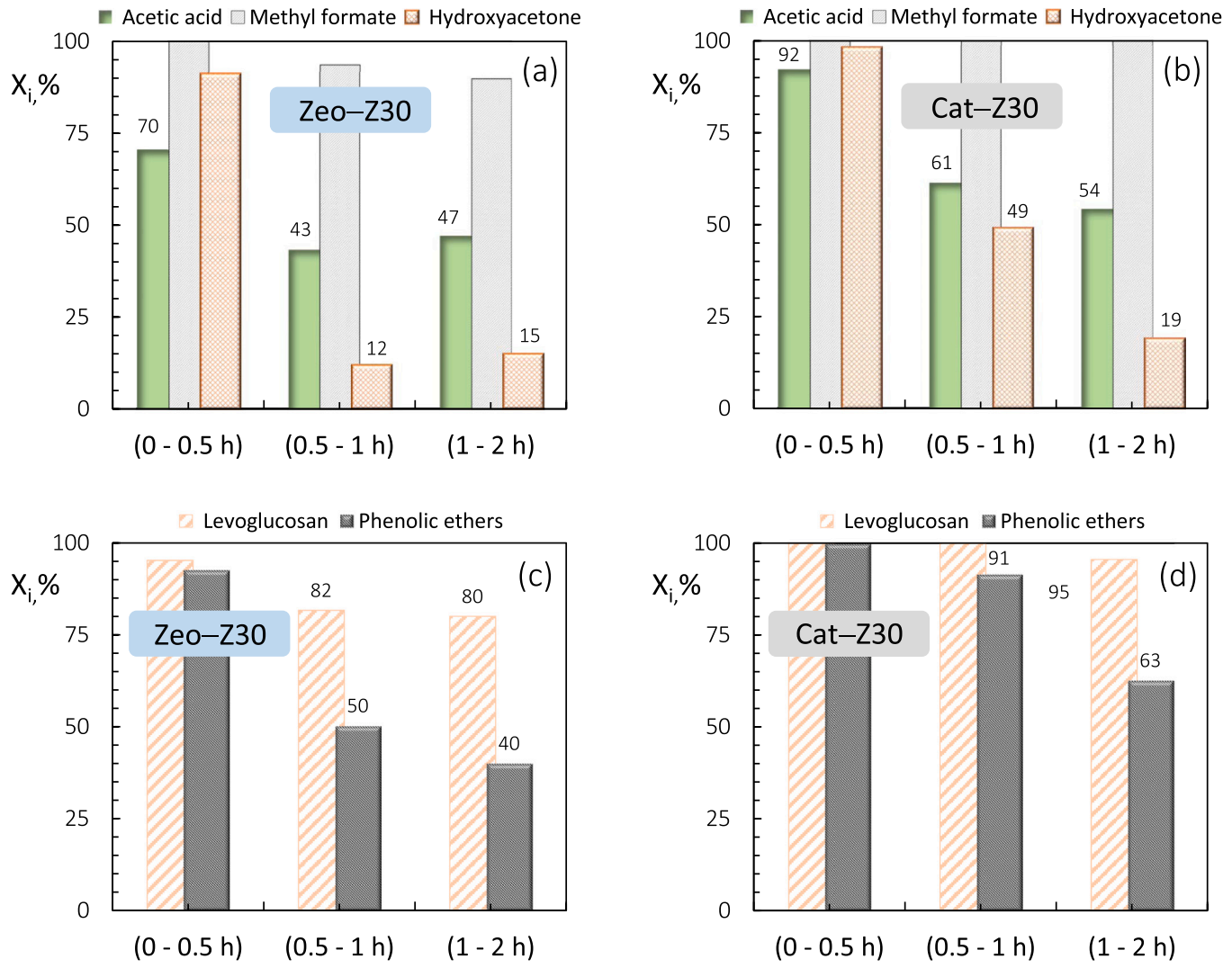


**Fig. 2.** Comparison of the evolution with time on stream of the individual conversion of oxygenates in the bio-oil using bulk HZSM-5 (Zeo−Z30) and alumina-embedded HZSM-5 (Cat−Z30). Acetic acid, methyl formate, hydroxyacetone (a-b), levoglucosan and phenolic ethers (c-d).

these compounds. Thus, the Zeo−Z30 catalyst produces mainly alkyl-phenols (70 %) and catechols (9 %), whereas the phenols detected with Cat−Z30 are mainly alkyl-phenols (73 %) and catechols (25 %). This fact suggests that decomposition of guaiacols by demethylation (DME) to form catechols (which undergo further dehydration into alkyl-phenols) is promoted when the alumina matrix is present [47].

Based on these results, the following conversion order can be established on the alumina-embedded Cat-Z30 catalyst: levoglucosan ≈ methyl formate > phenolic ethers > acetic acid > hydroxyacetone. Our results are in line with other reported on the reactivity of these compounds, with the exception of phenolic ethers which showed poor conversion [48–50]. This difference can be explained by the fact that the methanol contained in the feed (whose individual conversion is shown in Fig. 1b) may act as an hydrogen donor, promoting guaiacol dehydroxylation and alkylation (methylation) reactions [51].

It is worth mentioning that the liquid product collected when the Cat−Z30 catalyst activity for hydrocarbon formation is almost negligible (above 1 h, Fig. 1) should not be considered as a wastewater stream because it could be even more interesting than the bio-oil itself for some applications. Indeed, the composition of the aqueous fraction collected in the 1–2 h range (35 wt. % water, 19 wt. % unreacted methanol, 46 wt. % bio-oil derived oxygenates) is suitable for the sustainable production of $H_2$ by steam reforming. The high-water content would reduce the need of additional water supply to operate at suitable steam/carbon (S/C) ratio. Its composition is characterized by a high content of hydroxyacetone and acetone (10 %), acetic acid (8 %), methyl-acetate (7 %), and dimethyl-acetal (5 %), which account for more than 65 % of the oxygenates. Acetone is likely produced by ketonization of acetic acid and decomposition of hydroxyacetone (via intermediate acetic acid), and methyl acetate is produced by esterification of acetic acid with methanol. The low concentration of phenolic ethers (< 1 %) is also especially appealing because these compounds cause a rapid catalyst deactivation by coke deposition in the steam reforming of raw bio-oil [52]. In this context, the combination of catalytic cracking and steam reforming for producing hydrocarbons and hydrogen would be an attractive approach that enables the integral valorization of bio-oil. In addition, the chemicals-enriched composition of the liquid byproduct, particularly methyl ketones and carboxylic acids, makes it also attractive for the extraction of fine chemicals [53]. This way, the co-production of hydrocarbon fuels and high-value chemicals would improve the bio-oil valorization efficiency and the economic viability within a multi-product biorefinery concept [54,55].

In order to assess the effect of the alumina matrix on the distribution of liquid $C_{5+}$ hydrocarbons, the evolution with time on stream of the yield of each constituent lump ($Y_i$) is compared in Fig. 3. These lumps studied are BTEX (benzene, toluene, ethylbenzene, xylenes), $C_5$−$C_{12}$ (alkylbenzenes, naphthalenes, and aliphatics), and heavy $C_{12+}$ poly-aromatics (PAHs).

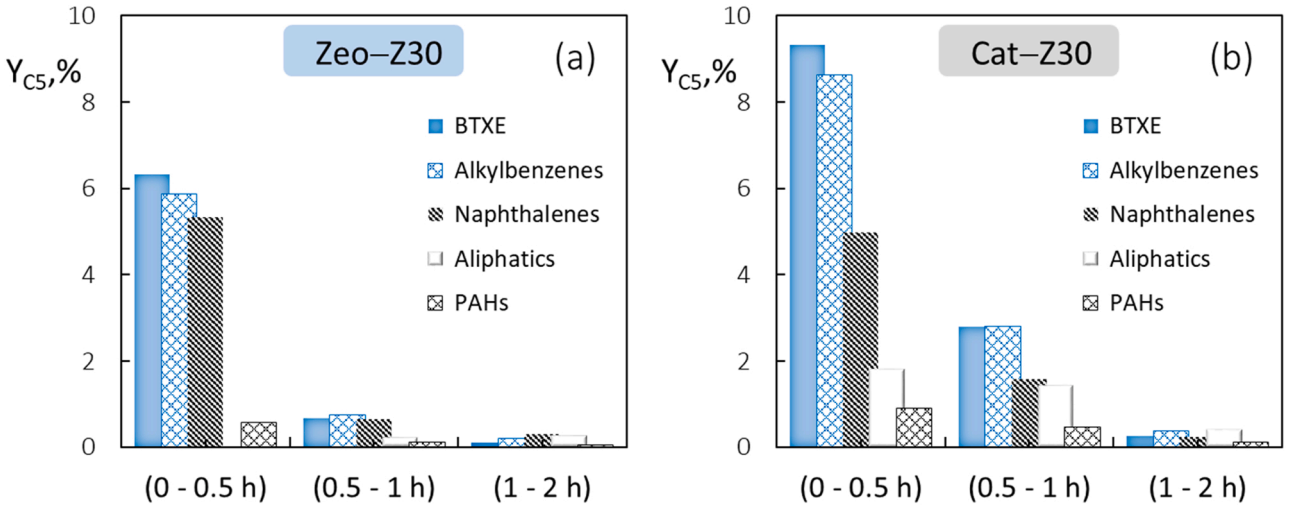


**Fig. 3.** Comparison of the evolution with time on stream of the yield of each $C_{5+}$ constituent lump: BTXE (benzene, toluene, ethylbenzene, xylenes), alkylbenzenes, naphthalenes, aliphatics, and $C_{12+}$ poliaromatics (PAHs) using bulk HZSM-5 (Zeo–Z30) and alumina-embedded HZSM-5 (Cat–Z30).

Due to the lower deactivation rate caused by the presence of the matrix (Fig. 1), the cumulative yield of $C_{5+}$ hydrocarbons obtained in the 0–0.5 h range with Cat–Z30 was 26 % (Fig. 3b), which is notably higher than that produced with Zeo–Z30 (18 %) (Fig. 3a). Regarding the yield of each constituent lump, the Cat–Z30 catalyst enhanced the production of $C_5$–$C_{12}$ MAH monoaromatic hydrocarbons (BTEX and other alkylbenzenes) to a greater extent than naphthalenes. Also noticeable was the 2 % yield of aliphatic hydrocarbons (mainly linear olefins), which were negligible with Zeo–Z30 catalyst. This significant difference is also maintained in the 0.5–1 h range.

Considering that space-time referred to HZSM-5 zeolite was the same (0.35 $g_{zeolite}$ h $g_{feed}^{-1}$), the amount of active acid sites provided in both runs corresponding to Fig. 3 was similar. Therefore, the greater production of gasoline-range MAH and aliphatic hydrocarbons attained with Cat-Z30 catalyst can be solely attributed to the presence of γ-$Al_2O_3$/α-$Al_2O_3$ matrix. It provides a weak-acid mesoporous structure that facilitates the conversion pathways involving bulky bio-oil molecules (such as saccharides and phenolic ethers), promoting their primary cracking/deoxygenation reactions (mainly dehydration). Furthermore, the zeolite crystals are homogeneously embedded in the matrix so that the accessibility of bulky oxygenates to the acid sites located on the external surface is improved. The conversion of light oxygenates (such as acetic acid and hydroxyacetone) is also enhanced by promoting their diffusion to the acid sites located in the micropores (*diffusive* role). Furthermore, the mesoporous structure seems to promote the diffusion of gasoline-range MAHs and aliphatic olefins outwards the zeolite crystals, boosting the production of these hydrocarbons (*spread* role).

### 3.2. Role of alumina matrix on coke deposition

In this section, the assessment of the role that the γ-$Al_2O_3$/α-$Al_2O_3$ matrix plays on the coke deposition will be exposed. The combination of the different techniques, (described in Section 2.2) applied to analyze Zeo–Z30 and Cat–Z30 deactivated catalysts allows to gain knowledge on content, nature and location of coke species. Firstly, the results obtained by TPD-TPO, $N_2$ physisorption, and $NH_3$-TPD will be shown, which give information on the content and nature of the coke and its effect on the deterioration of the physico-chemical properties of the catalyst. Then, we give a comprehensive fingerprint of the coke species deposited by using the TPD-GC/MS technique to analyze the composition of the most easily removable coke species (*soft coke*), and a high-resolution spectrometry technique (LDI FT-ICR MS) to analyze the composition of the most complex and evolved coke (*hard coke*).

#### 3.2.1. Content and nature of coke

The complete TPD-TPO profile of Cat–Z30 sample (after 2 h on stream) is depicted in Fig. 4 as an example. The coke species released in the desorption stage with $N_2$ (TPD) were accounted as *soft coke*, and the remaining coke species released during combustion stage (TPO) were accounted as *hard coke*.

Three runs with the same operating conditions but different durations (0.5, 1, and 2 h) were carried out with both catalysts, with the aim of studying the effect of alumina matrix on the evolution of coke deposition with time on stream. The corresponding TPD-TPO results of deactivated catalyst samples are gathered in Fig. 5, where the removal of the *soft coke* (TPD profiles) (Fig. 5a) and the *hard hoke* (TPO profiles) (Fig. 5b) are compared separately. It should be noted that the results are shown per mass unit of catalyst, so the coke contents per mass unit of zeolite would be double on Cat-Z30 catalyst. The resulting values of total coke content are displayed in Table 2, and the evolutions with time on stream of the content of *soft coke* and *hard coke* deposited on each catalyst are compared in Fig. 6.

Two distributions were clearly identified in the TPD profiles for both catalysts, which were ascribed to a *low temperature–soft coke (LT-SC)* and *high temperature–soft coke (HT-SC)* (Fig. 5a). No clear differences were observed in the content of *LT-SC* fraction deposited on both catalysts, thus pointing to volatile compounds retained on the external surface that are easily removed under $N_2$ flow at low temperatures (below 200 °C). In the case of *HT-SC* coke species released at higher

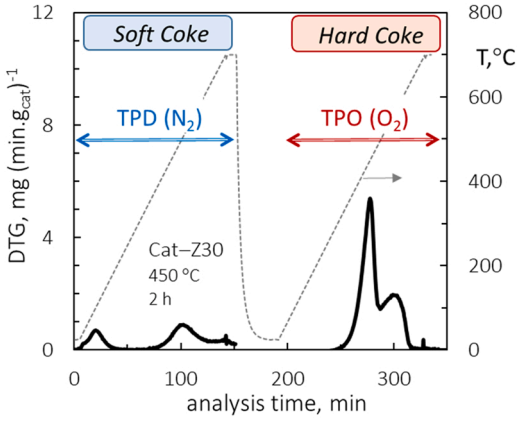


**Fig. 4.** Example of complete TPD-TPO analysis of spent catalyst (Cat–Z30 after 2 h reaction).

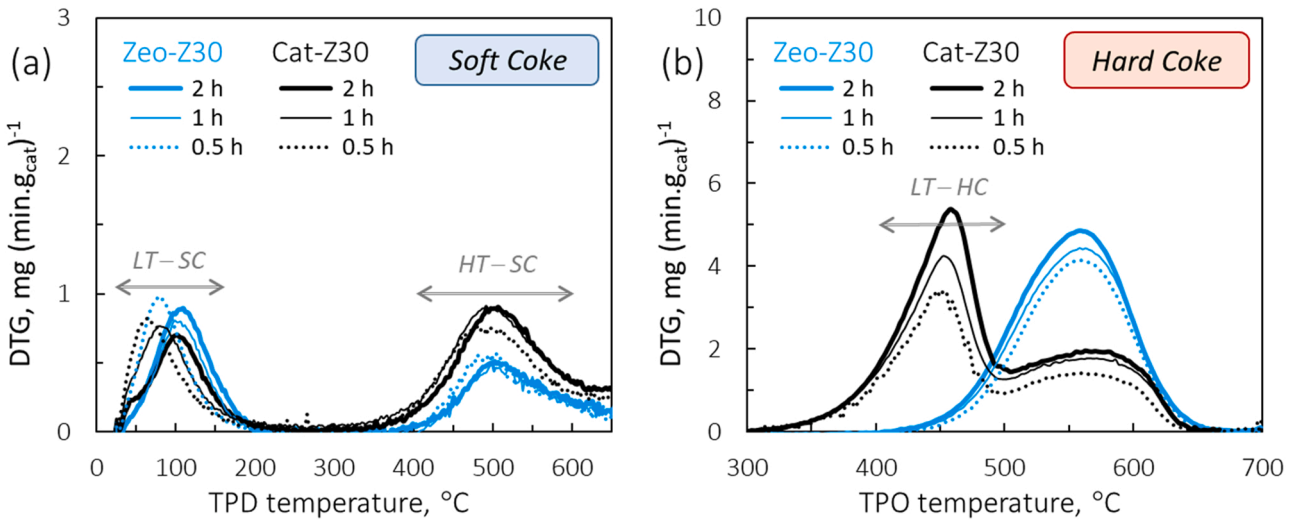


**Fig. 5.** Comparison of the evolution with time on stream of the *soft coke* (TPD profiles, a) and *hard coke* (TPO profiles, b) deposited on both catalysts.

**Table 2**
Total coke content on each catalyst for different values of time on stream.

| | 0.5 h | 1 h | 2 h |
|---|---|---|---|
| Zeo−Z30 | 129 | 134 | 142 |
| Cat−Z30 | 128 | 155 | 171 |

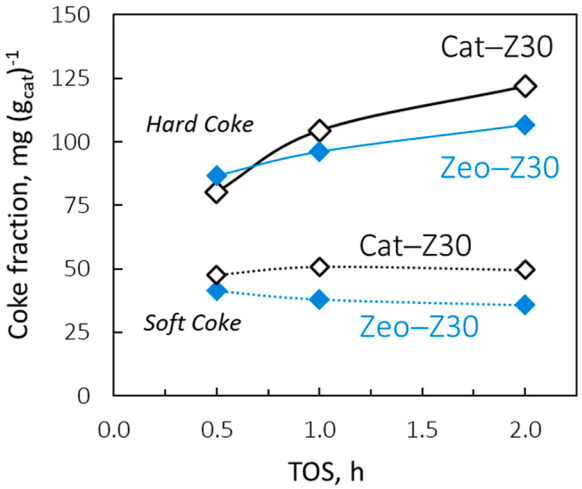


**Fig. 6.** Comparison of the evolution with time on stream of the content of each coke fraction on both catalysts. *soft coke* (dotted lines) and *hard coke* (solid lines).

temperature (maximum rate at 500 °C) greater amount was observed for Cat−Z30 in comparison with Zeo−Z30 catalyst. The species removed during the TPD of zeolite catalysts deactivated in the cracking of hydrocarbons [56] and methanol-to-olefins (MTO) reactions [57] have been previously ascribed to coke precursors. However, these species could be also the consequence of the *aging* (dehydrogenation and decomposition reactions) that *hard coke* may undergo under $N_2$ atmosphere at high temperature [58]. Therefore, the limited information provided by the TPD will be complemented by spectrometric analyses for identifying the nature of such species (Section 3.2.3).

After the TPD, the remaining heavier aromatic species (*hard coke*) were eventually removed by combustion. The TPO profiles, compared in Fig. 5b, reveal clear differences between both catalysts. All deactivated samples of bulk Zeo−Z30 catalyst have a wide yet unique combustion peak in the 450–650 °C range. The coke content is remarkable even at low values of TOS, which would explain the rapid loss of catalyst activity (Fig. 1) and points to the highly deactivating nature of this coke. The great amplitude of the ill-defined combustion peak gives evidence on its heterogeneous nature, caused by the complex mixture of oxygenates present in the real bio-oil feed. Our results are in line with most literature dealing with deactivation of zeolites in the catalytic conversion of raw bio-oil, which recognizes both thermal (polymerization of oxygenates) and catalytic (condensation-growth of aromatic precursors) as the main pathways involved in the formation of coke [59–61]. Even the impact of the oxygenated functional group on the amount and/or combustion dynamics of the coke deposited on HZSM-5 zeolite has become evident by the numerous studies on the individual conversion into hydrocarbons of bio-oil model compounds. For instance, Chen et al. [49] reported a single combustion peak for guaiacol and acetic acid (at ca. 460 °C and 560 °C, respectively) whereas acetol and furfural showed two-peak TPO profile each with combustion temperatures varying in a range over 50 °C.

Interestingly, the TPO profiles of Cat−Z30 samples (Fig. 5b) show two clear combustion domains, with an additional peak appearing in the 400–500 °C range, corresponding to *low temperature−hard coke* (*LT-HC*). This coke fraction is likely deposited on the mesoporous structure of the matrix, which would favor its combustion, resulting in lower and narrower range of temperatures compared with the coke species deposited on the zeolite crystals. The continuous growth of *LT-HC* even when Cat−Z30 is practically deactivated for hydrocarbons formation (above 1 h on stream, Fig. 1c) points to an origin associated with the polymerization of phenolic compounds, which agrees with the lower conversion of phenolic ethers (Fig. 2d). Because of the growth of this *LT-HC* coke fraction in the matrix, the total coke content on Cat-Z30 increases more markedly with time n stream, in contrast to Zeo-Z30 catalyst that shows a smoother trend (Fig. 6).

These results reveal that the alumina matrix has a great impact on the content and nature of the coke deposited on HZSM-5 zeolite, which explains the difference in deactivation dynamics of Cat-Z30 catalyst. The relationship between TPD-TPO results and catalyst behavior (Fig. 1) evidences the lower deactivating nature of the coke species deposited on the matrix (*LT-HC*), which is the prevailing fraction on Cat-Z30 (Fig. 5b). Although these TPD-TPO profiles provide useful information on the content and nature of the coke this technique needs to be complemented in order to gain knowledge on location and composition of deactivating coke species.

### 3.2.2. Physico-chemical properties of deactivated catalysts

In this section, the deterioration of physico-chemical properties caused by the deposition of coke on each catalyst is displayed. The evolution of textural properties (BET surface area and micropore volume) and residual acidity with the total coke content are compared in Fig. 7. Despite the properties of both catalysts exhibit the expectable decreasing trends, there are clear differences attributable to the coke species impact on the zeolite pore blockage. Thus, the coke deposited on Zeo−Z30 catalyst causes a faster blockage of micropores, evidenced by the significant loss of textural properties (above 95 % of the initial values in 0.5 h on stream). The BET surface area plunges from 428 $m^2.g^{-1}$ to 26 $m^2.g^{-1}$ (Fig. 7a) and the micropore volume decreases from 0.17 $m^3.g^{-1}$ to almost negligible values (Fig. 7b). In comparison, the Cat−Z30 catalyst undergoes less severe micropore blockage, with the BET surface area decreasing by ca. 65 % of the initial value (fresh catalyst) and micropore volume by ca. 60 %. Besides, this catalyst maintains residual values of surface area (80 $m^2g^{-1}$) and micropore volume (0.02 $m^3g^{-1}$) even for high coke contents. The values of acidity (Fig. 7c) show trends in line with the decrease of microporous properties.

These results qualitatively quantify the deterioration of the catalyst porous structure and are consistent with the deactivation rates (Fig. 1). The highly heterogeneous coke deposited on bulk zeolite Zeo−Z30 catalyst causes a rapid blockage of micropore channels, thus hindering the access of reactants to the active sites. In comparison, the coke deposited on the alumina-embedded Cat−Z30 catalyst causes a lower blockage of micropores. This fact evidences that these coke species (ascribed to *LT-HC*, Fig. 5b) are effectively deposited within the mesoporous structure of the matrix, causing less impact on deactivation.

### 3.2.3. Composition of soft coke (TPD-GC/MS)

The TPD-GC/MS technique (described in Section 2.2.3) was applied to analyze the composition of the so-called *soft coke*, which accounts for the coke species removable under inert gas flow at two temperature ranges (Fig. 5a). Fig. 8 shows the averaged values obtained for the composition of the *low temperature soft coke* (*LT-SC*) and *high temperature soft coke* (*HT-SC*) deposited on both catalysts because no significant differences were detected between them for a given coke fraction. The similarity of results evidence that the presence of $\gamma$-$Al_2O_3$/$\alpha$-$Al_2O_3$ matrix does not affect the composition of *soft coke*, suggesting that this is related to coke species deposited on the external surface of catalyst particles and zeolite crystals. Nevertheless, the coke fractions do differ significantly from each other. The *LT-SC* fraction is mainly composed of $C_5$−$C_{15}$ linear chains containing oxygenated functionalities, named *Alkyl-Oxygenates*. The major compounds detected are long-chain aldehydes (e.g., nonanal), acids (e.g., pentadecanoic acid), and alcohols (e.g., 2-butyl-1-octanol). In addition, low amounts of aromatics containing oxygenated groups (*Aryl-Oxygenates*) and aliphatic hydrocarbons were

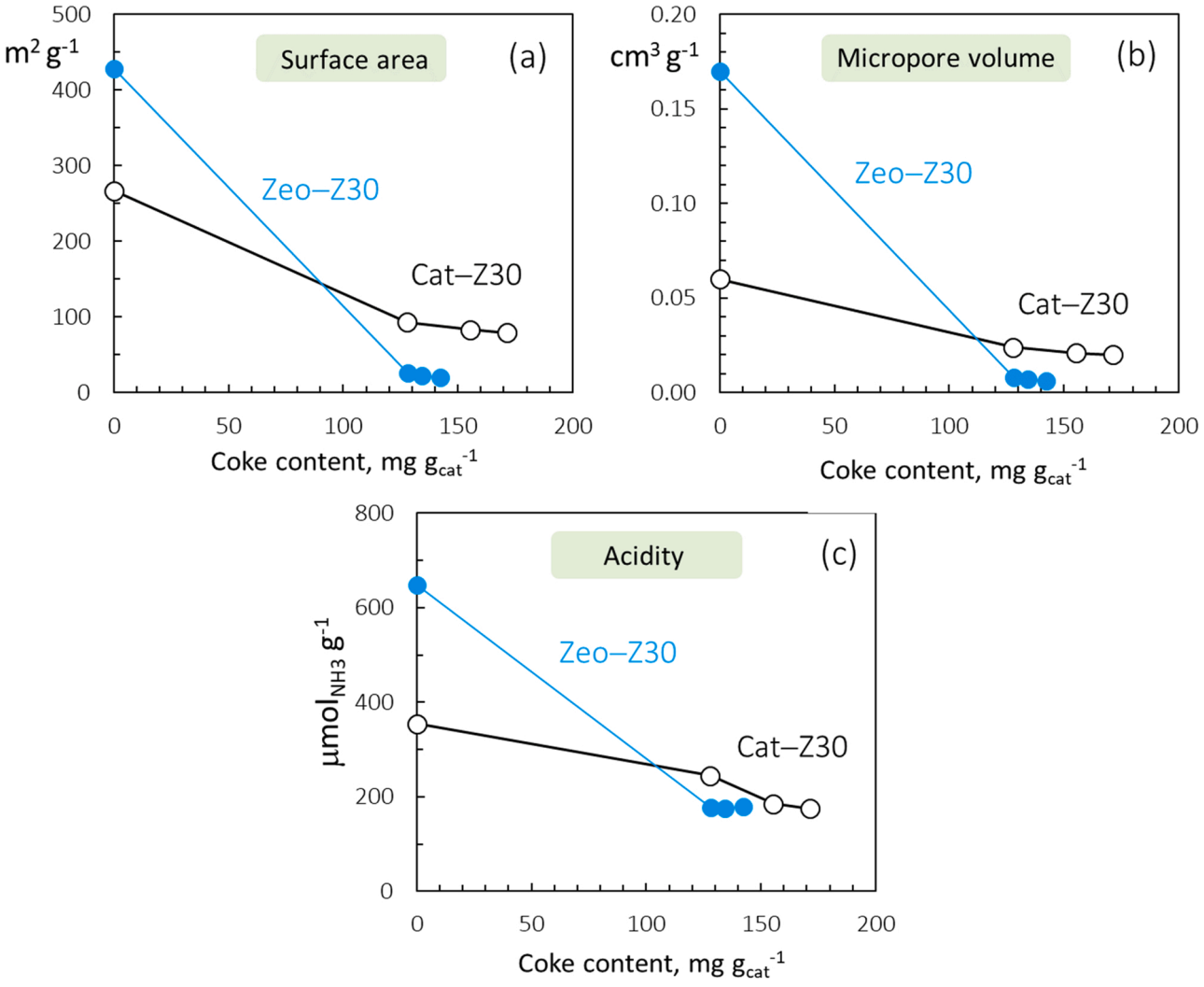


**Fig. 7.** Comparison of the evolution with the total coke content of surface area (a), micropore volume (b), and total acidity (c) of bulk HZSM-5 (Zeo−Z30) and alumina-embedded HZSM-5 (Cat−Z30) catalysts.

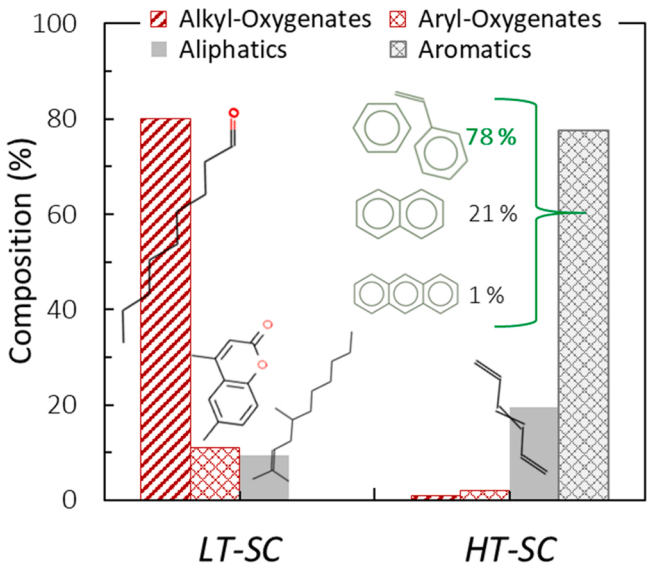


**Fig. 8.** Composition of low-temperature soft coke (*LT–SC*) and high-temperature soft coke (*HT–SC*) deposited on both catalysts (deactivated after 2 h on stream).

detected. Conversely, the *HT-SC* fraction has a very different composition, with negligible content of oxygenated functionalities and aromatic hydrocarbons being the prevailing species (Fig. 8). Significant content (ca. 20 %) of $C_5$–$C_{10}$ aliphatic hydrocarbons (mainly linear olefins) was also detected.

The prevailing oxygenate nature of *LT-SC* fraction containing long-chain aliphatic structures points that these coke species are formed by chain-growth (polymerization) reactions of bio-oil oxygenates, which are mainly retained on the external surface of the zeolite crystals. The aromatic nature of *HT-SC* fraction, with majority of cyclic aromatics (78 %) (Fig. 8) suggests that it is mainly composed of active coke precursors located in the zeolite micropores. The bicyclic rings detected (21 % of aromatics) presumably come from the polymerization of these active species, which may also lead to linear polycyclic aromatics (anthracene) within the micropore channels and crystal surface, eventually blocking the access to the acid sites [62]. It is worth noting that the release of light aromatics (mono and bicyclic structures) during coke aging under an inert atmosphere may be linked to changes in coke composition [58]. Hence, contribution of the most evolved *hard coke* to these aromatics cannot be ruled out.

### 3.2.4. Composition of hard coke (LDI FT-ICR MS)

This technique (described in Section 2.2.3) was applied to analyze the *hard coke* composition, which accounts for the most complex and evolved coke species. In order to avoid disturbance in the results, the LDI FT-ICR MS analyses were conducted after removing the *soft coke*. The Zeo–Z30 analysis provides straightforward information of the coke species deposited on the bulk zeolite crystals, and the differences with Cat–Z30 are attributable to the coke species deposited in the alumina matrix (*LT–HC*), which is the predominant fraction in this catalyst. The results are gathered in Fig. 9.

The ion mass spectrum of Zeo–Z30 (Fig. S2) reveals a neater distribution of species, with 317 assignments compared with that of Cat–Z30, which exhibits a larger number of peaks along the 100–1500 Da range (1086 molecular assignments) indicating the

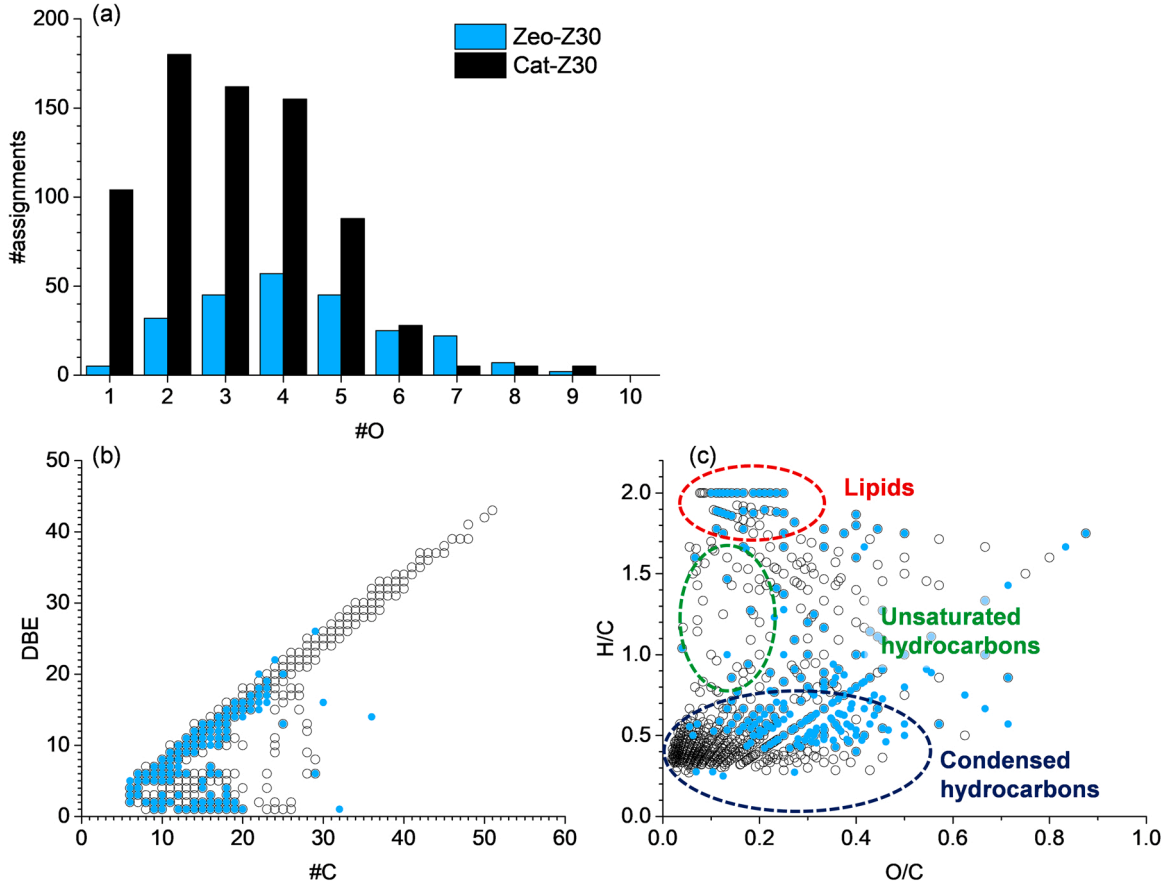


**Fig. 9.** Results of (a) O-distribution, (b) DBE vs. carbon number graph, and c) van Krevelen diagram of $CHO_x$ compounds detected by LDI FT-ICR MS analyses of the *hard coke* deposited on both catalysts (deactivated after 2 h on stream).

presence of a wider variety of deactivating species. These species in Cat−Z30 catalyst are ascribed to $CHO_X$ compounds (67 %), CH (14 %), $CHSO_X$ (10 %), $CHAlO_X$ (8 %), and C (1 %). The resulting distribution of species in Zeo−Z30 catalyst is $CHO_X$ (76 %), $CHSO_X$ (16 %), CH (1 %), $CHAlO_X$ (5 %), and C (2 %). The $CHSO_X$ are regular contaminants in negative-ion mode and the $CHAlO_X$ species can be complex of alumina from the catalyst and organic compounds. Pure hydrocarbon CH species might be the result of recombination processes occurring during the laser–matter interaction at high irradiance and, consequently, they should not be considered to be specific of the sample [30].

One finding that can be drawn from the LDI FT-ICR MS results is the oxygenated nature of the *hard coke*, evidenced by the significant content of $CHO_X$ species, with clear differences between both catalysts. The distribution of $CHO_X$ molecular assignments as a function of oxygen atom counts (Fig. 9a) show that the $CHO_X$ species contained in Zeo−Z30 catalyst are overall more oxygenated (with distribution centered at four oxygen atoms) compared with Cat−Z30 species, with a distribution centered at two oxygen atoms. These results are in agreement with the *diffusive* role of the matrix (discussed in Section 3.1), which enhances the fragmentation/deoxygenation of bulky bio-oil oxygenates, which otherwise would polymerize on the zeolite crystals. This role entails that the $CHO_X$ species identified in Cat−Z30 catalyst have a lower average oxygen content than the molecules deposited on Zeo−Z30, formed by polymerization/condensation of bio-oil oxygenates on the zeolite crystals, blocking access to active sites. In addition, the matrix provides a mesoporous structure that favors the development of this thermally-induced coke away from the micropores (*shell* role), as evidenced by the notably higher content of $CHO_X$ compounds in Cat−Z30 (Fig. 9a).

The van Krevelen diagram (Fig. 9c) gives straightforward information of the content of different types of compounds, such as unsaturated and condensed hydrocarbons, and lipid-like molecules. By comparing both catalysts, the greater content of condensed hydrocarbons on Cat−Z30 catalyst (ascribed to large polycyclic aromatics characterized by low O/C and H/C ratios) is clearly revealed. Also noteworthy is the content of lipid-like compounds detected. These structures can be also ascribed to long-chain oxygenates, which is consistent with the alkyl-oxygenates ($C_5$−$C_{15}$ aldehydes and acids) identified in the *low-temperature soft coke* (*LT-SC*) by TPD-GC/MS technique (Fig. 8). Our results are consistent with previous reports on the presence of O-containing aliphatic structures in the coke, which is primarily ascribed to a *thermal coke* (or pyrolytic lignin) formed by polymerization of bio-oil compounds [59,61,63].

The DBE (double bound equivalent) values that represent the unsaturation degree (aromaticity) of compounds in the *hard coke* were depicted as a function of the number of carbon atoms, which represents the alkylation degree (Fig. 9c). By comparing the results for both catalysts, the heavier nature and higher unsaturation degree of the *hard coke* deposited on Cat−Z30 catalyst is clearly revealed. In this catalyst, the coke species reach DBE values close to 45 and the average number of carbon atoms ranges from 6 (single benzyl rings) up to 52 (ascribable to polycyclic aromatics containing eight-nine rings). In contrast, the *hard coke* species deposited on the Zeo-Z30 catalyst reach a maximum DBE values of ca. 20 and a maximum number of carbon atoms of ca. 24 (corresponding to four aromatic ring structures). These results are in agreement with the *spread* role of the matrix (discussed in Section 3.1), which enhances the diffusion of olefins and MAHs (precursors of *hard coke*) outwards the zeolite crystals. The alumina matrix provides a mesoporous structure that enables further aromatization-condensation reactions of coke precursors, leading to the formation of heavy poly-aromatic coke species away from the micropores, growing outwards (*growth* role). The polymerization of phenolic compounds within the matrix, especially phenolic ethers (Fig. 2d), may well contribute to these aromatic coke species, which would explain the growth of the *low temperature hard coke* (*LT−HC*) even when the Cat−Z30 is deactivated for hydrocarbon formation (Fig. 5b). Our results are in good concordance with those reported by authors identifying different dynamics of coke formation during the catalytic conversion of raw bio-oil, such as thermally-induced deposition (as so-called thermal lignin, thermal coke, pyrolytic lignin, etc.) and catalytically-induced deposition by aromatics condensation [59,60,64,65].

The results discussed in this work evidence that embedding the bulk HZSM-5 zeolite within a $\gamma$-$Al_2O_3$/$\alpha$-$Al_2O_3$ matrix is an effective strategy for attenuating the severe deactivation that this microporous zeolite undergoes in the catalytic cracking of raw bio-oil. This advantageous effect is attributed to its weak-acid mesoporous structure, which promotes diffusion and the primary cracking of bulky oxygenates and plays an important role in coke deposition. Thus, the matrix provides a mesoporous structure in which both thermal-induced coke and catalytic coke develop away from the active sites located in micropores, thereby delaying their blockage. Scheme 1 summarizes the composition of the different types of coke identified and their prevailing location. For the sake of clarity, a tentative molecular depiction of the role that the alumina matrix plays in the dynamics of coke deposition is proposed in Scheme 2.

## 4. Conclusions

The agglomeration of microporous HZSM-5 zeolite with a mesoporous $\gamma$-$Al_2O_3$/$\alpha$-$Al_2O_3$ matrix was proved a simple, low-cost and effective method for preparing an attrition-resistant catalyst with extended lifetime for cracking of real bio-oil feedstock (raw bio-oil stabilized with 20 wt. % of methanol). The matrix enhanced the accessibility of bulky molecules (e.g., saccharides and guaiacols) to the acid sites on the external surface of the zeolite crystals, promoting their fragmentation/deoxygenation (primary cracking) into light reactive oxygenates (e.g., acetic acid and hydroxyacetone) that access the acid sites in the zeolite micropores.

The role of the matrix was clearly evidenced by the improvement of oxygenates conversion and hydrocarbon yields. The alumina-embedded catalyst (Cat-Z30) exhibited greater stability, keeping the bio-oil conversion above 88 % and methanol conversion above 93 % for 0.5 h at the operating conditions (450 ºC, 0.35 $g_{zeolite}.h.g_{feed}^{-1}$). In comparison, the bulk HZSM-5 underwent rapid deactivation showing a sharp decrease in the conversion of bio-oil (from 95 % to 40 %) and methanol (from 97 % to 60 %). Consequently, the cumulative yield of $C_{5+}$ hydrocarbons (with more than 70 % BTXE and alkylbenzenes) was boosted from 18 % to 26 % for the same reaction time. In addition, the Cat-Z30 catalyst reached a pseudo-steady state (remaining activity for dehydration/deoxygenation reactions), which led to a concurrent production of aqueous liquid byproduct with suitable composition for $H_2$ production by further steam reforming. This combined approach would be interesting to progress towards the integral valorization of raw bio-oil in bio-refinery.

The enhanced behavior of Cat-Z30 was explained by the role of the weak-acid mesoporous structure of the matrix in attenuating the deactivation by coke, which was extensively investigated by $N_2$ physisorption, $NH_3$-TPD, TPD-TPO, TPD-GC/MS and LDI FT-ICR MS. The combination of techniques provided insights on the content, composition and prevailing location of coke species, evidencing the dual function of the matrix: i) *Diffusive-shell* (inwards) enhancing the development of thermally-induced coke (formed by polymerization of oxygenates) away from the zeolite micropores; ii) *Spread-growth* (outwards) promoting diffusion of MAHs and olefins outwards the zeolite crystals and the development of heavy polycyclic structures (*hard coke*) away from the micropores, thereby delaying the blockage of active sites.

The results of this work provide insights on the content, nature and prevailing location of coke deposited on HZSM-5 zeolite, and thereby on the formation and growth of deactivating coke species. This knowledge is essential to address the design of reaction-regeneration strategies to optimize the catalyst efficiency when dealing with complex feedstock such bio-oil. The beneficial effect of including a mesoporous matrix in the catalyst design also offers opportunities for future research aimed at improvement structure/acidity of the matrices.

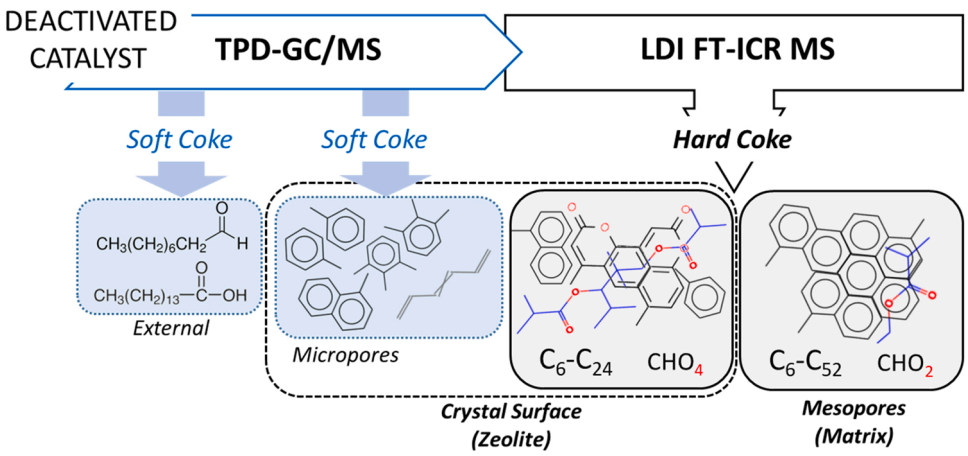


**Scheme 1.** Summary of the composition and location of coke species determined by combining TPD-GC/MS and LDI FT-ICR MS spectroscopic techniques.

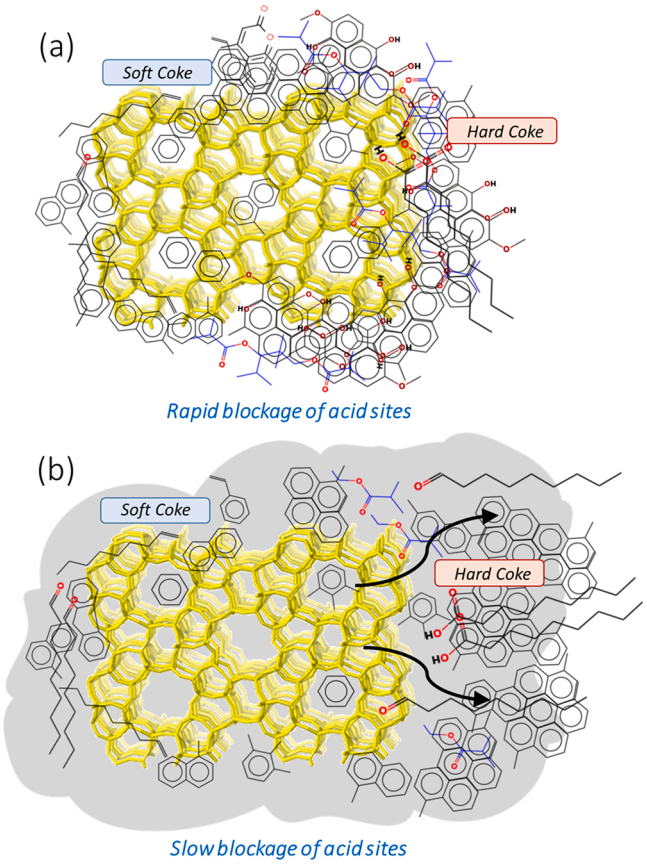


**Scheme 2.** Molecular level description of the dynamics of coke deposition on (a) bulk HZSM-5 (Zeo-Z30) and (b) alumina-embedded HZSM-5 (Cat-Z30).

## CRediT authorship contribution statement

**Iratxe Crespo**: Investigation, Formal analysis, Visualization, Writing−Original Draft **Jasmine Hertzog**: Investigation, Methodology, Visualization, Writing−Original Draft, Writing−Review & Editing **Vincent Carré**: Investigation, Methodology, Visualization **Frédéric Aubriet**: Investigation, Methodology, Visualization **Beatriz Valle**: Conceptualization, Methodology, Investigation, Formal analysis, Writing−Original Draft, Writing−Review & Editing, Supervision, Project administration, Funding acquisition.

## Declaration of Competing Interest

None declared.

## Data Availability

The authors are unable or have chosen not to specify which data has been used.

## Acknowledgements

This work was supported by the Ministry of Science and Innovation of the Spanish Government (grant number RTI2018–095990-J-I00 funded by MCIN/AEI/10.13039/501100011033 and by "ERDF A way of making Europe"); Department of Education, Universities and Investigation of the Basque Government (Project IT1645-22); University of the Basque Country (grant UPV/EHU PIF 2021 of Iratxe Crespo). Financial support from the IR INFRANALYTICS FR2054 for conducting the research is gratefully acknowledged.

## Appendix A. Supporting information

Supplementary data associated with this article can be found in the online version at doi:10.1016/j.jaap.2023.106009.

## References

[1] A.B. Culaba, A.P. Mayol, J.L.G. San Juan, C.L. Vinoya, R.S. Concepcion, A. A. Bandala, R.R.P. Vicerra, A.T. Ubando, W.H. Chen, J.S. Chang, Smart sustainable biorefineries for lignocellulosic biomass, Bioresour. Technol. 344 (2022), 126215, https://doi.org/10.1016/J.BIORTECH.2021.126215.
[2] L. Dai, N. Zhou, H. Li, W. Deng, Y. Cheng, Y. Wang, Y. Liu, K. Cobb, H. Lei, P. Chen, R. Ruan, Recent advances in improving lignocellulosic biomass-based bio-oil production, J. Anal. Appl. Pyrolysis 149 (2020), 104845, https://doi.org/10.1016/J.JAAP.2020.104845.
[3] H.A. Baloch, S. Nizamuddin, M.T.H. Siddiqui, S. Riaz, A.S. Jatoi, D.K. Dumbre, N. M. Mubarak, M.P. Srinivasan, G.J. Griffin, Recent advances in production and upgrading of bio-oil from biomass: a critical overview, J. Environ. Chem. Eng. 6 (2018) 5101–5118, https://doi.org/10.1016/J.JECE.2018.07.050.
[4] B. Valle, A. Remiro, N. García-Gómez, A.G. Gayubo, J. Bilbao, Recent research progress on bio-oil conversion into bio-fuels and raw chemicals: a review, J. Chem. Technol. Biotechnol. 94 (2019) 670–689, https://doi.org/10.1002/jctb.5758.
[5] F. Lin, M. Xu, K.K. Ramasamy, Z. Li, J.L. Klinger, J.A. Schaidle, H. Wang, Catalyst deactivation and its mitigation during catalytic conversions of biomass, ACS Catal. 12 (2022) 13555–13599, https://doi.org/10.1021/acscatal.2c02074.
[6] N. Le-Phuc, P.T. Ngo, Q.L.M. Ha, T.V. Tran, T.T. Phan, L.C. Luu, L.T. Duong, B.M. Q. Phan, Efficient hydrodeoxygenation of guaiacol and fast-pyrolysis oil from rice straw over PtNiMo/SBA-15 catalyst for co-processing in fluid catalytic cracking process, J. Environ. Chem. Eng. 8 (2020), 103552, https://doi.org/10.1016/J.JECE.2019.103552.
[7] Á. Ibarra, E. Rodríguez, U. Sedran, J.M. Arandes, J. Bilbao, Synergy in the cracking of a blend of bio-oil and vacuum gasoil under fluid catalytic cracking conditions,

Ind. Eng. Chem. Res. 55 (2016) 1872–1880, https://doi.org/10.1021/acs.iecr.5b04502.
[8] D.M. Santosa, I. Kutnyakov, M. Flake, H. Wang, Coprocessing biomass fast pyrolysis and catalytic fast pyrolysis oils with vacuum gas oil in refinery hydroprocessing, Energy Fuels 36 (2022) 12641–12650, https://doi.org/10.1021/acs.energyfuels.2c02367.
[9] S. Hansen, A. Mirkouei, L.A. Diaz, A comprehensive state-of-technology review for upgrading bio-oil to renewable or blended hydrocarbon fuels, Renew. Sustain. Energy Rev. 118 (2020), 109548, https://doi.org/10.1016/j.rser.2019.109548.
[10] J. Liang, G. Shan, Y. Sun, Catalytic fast pyrolysis of lignocellulosic biomass: critical role of zeolite catalysts, Renew. Sustain. Energy Rev. 139 (2021), 110707, https://doi.org/10.1016/j.rser.2021.110707.
[11] B. Puértolas, A. Veses, M.S. Callén, S. Mitchell, T. García, J. Pérez-Ramírez, Porosity–acidity interplay in hierarchical ZSM-5 zeolites for pyrolysis oil valorization to aromatics, ChemSusChem 8 (2015) 3283–3293, https://doi.org/10.1002/cssc.201500685.
[12] Q. Cai, T. Yu, X. Meng, S. Zhang, Selective generation of aromatic hydrocarbons from hydrotreating-cracking of bio-oil light fraction with MOx modified HZSM-5 (M = Ga, Mo and Zn), Fuel Process. Technol. 204 (2020), 106424, https://doi.org/10.1016/j.fuproc.2020.106424.
[13] B. Valle, R. Palos, J. Bilbao, A.G. Gayubo, Role of zeolite properties in bio-oil deoxygenation and hydrocarbons production by catalytic cracking, Fuel Process. Technol. 227 (2022), 107130, https://doi.org/10.1016/J.FUPROC.2021.107130.
[14] H. Yang, T. Han, W. Yang, L. Sandström, P.G. Jönsson, Influence of the porosity and acidic properties of aluminosilicate catalysts on coke formation during the catalytic pyrolysis of lignin, J. Anal. Appl. Pyrolysis 165 (2022), 105536, https://doi.org/10.1016/J.JAAP.2022.105536.
[15] Y. Zheng, J. Wang, D. Wang, Z. Zheng, Advanced catalytic upgrading of biomass pyrolysis vapor to bio-aromatics hydrocarbon: A review, Appl. Energy Combust. Sci. 10 (2022), 100061, https://doi.org/10.1016/J.JAECS.2022.100061.
[16] A. Talebian-Kiakalaieh, S. Tarighi, Synthesis of hierarchical Y and ZSM-5 zeolites using post-treatment approach to maximize catalytic cracking performance, J. Ind. Eng. Chem. 88 (2020) 167–177, https://doi.org/10.1016/J.JIEC.2020.04.009.
[17] S. Mardiana, N.J. Azhari, T. Ilmi, G.T.M. Kadja, Hierarchical zeolite for biomass conversion to biofuel: a review, Fuel 309 (2022), 122119, https://doi.org/10.1016/J.FUEL.2021.122119.
[18] L.Y. Jia, M. Raad, S. Hamieh, J. Toufaily, T. Hamieh, M.M. Bettahar, G. Mauviel, M. Tarrighi, L. Pinard, A. Dufour, Catalytic fast pyrolysis of biomass: superior selectivity of hierarchical zeolites to aromatics, Green. Chem. 19 (2017) 5442–5459, https://doi.org/10.1039/C7GC02309J.
[19] S. Mitchell, N.L. Michels, J. Pérez-Ramírez, From powder to technical body: the undervalued science of catalyst scale up, Chem. Soc. Rev. 42 (2013) 6094–6112, https://doi.org/10.1039/C3CS60076A.
[20] M. Bertero, J.R. García, M. Falco, U. Sedran, Hydrocarbons from bio-oils: performance of the matrix in FCC catalysts in the immediate catalytic upgrading of different raw bio-oils, Waste Biomass. Valoriz. 8 (2017) 933–948, https://doi.org/10.1007/s12649-016-9624-z.
[21] M. Bertero, J.R. García, M. Falco, U. Sedran, FCC matrix components and their combination with Y Zeolite to enhance the deoxygenation of bio-oils, Bioenergy Res. 15 (2022) 1327–1341, https://doi.org/10.1007/S12155-021-10322-Z/FIGURES/2.
[22] N.-L. Michels, S. Mitchell, J. Pérez-Ramírez, Effects of binders on the performance of shaped hierarchical MFI zeolites in methanol-to-hydrocarbons, ACS Catal. 4 (2014) 2409–2417, https://doi.org/10.1021/CS500353B.
[23] P. Pérez-Uriarte, M. Gamero, A. Ateka, M. Díaz, A.T. Aguayo, J. Bilbao, Effect of the acidity of HZSM-5 zeolite and the binder in the DME transformation to olefins, Ind. Eng. Chem. Res. 55 (2016) 1513–1521, https://doi.org/10.1021/ACS.IECR.5B04477.
[24] M. Ibáñez, P. Pérez-Uriarte, M. Sánchez-Contador, T. Cordero-Lanzac, A.T. Aguayo, J. Bilbao, P. Castaño, Nature and location of carbonaceous species in a composite HZSM-5 zeolite catalyst during the conversion of dimethyl ether into light olefins, Catalysts 7 (2017) 254, https://doi.org/10.3390/catal7090254.
[25] C. Geantet, D. Laurenti, N. Guilhaume, C. Lorentz, I. Borghol, B. Bujoli, E. Chailleux, R. Checa, S. Schramm, V. Carré, F. Aubriet, C. Queffélec, FT-ICR MS characterization of bio-binders for road pavement from HTL of microalgae residues, J. Environ. Chem. Eng. 10 (2022), 107361, https://doi.org/10.1016/J.JECE.2022.107361.
[26] S. Cai, M. Liu, Y. Zhang, A. Hu, W. Zhang, D. Wang, Molecular transformation of dissolved organic matter and formation pathway of humic substances in dredged sludge under aerobic composting, Bioresour. Technol. 364 (2022), 128141, https://doi.org/10.1016/J.BIORTECH.2022.128141.
[27] N. Hassibi, Y. Quiring, V. Carré, F. Aubriet, L. Vernex-Loset, G. Mauviel, V. Burklé-Vitzthum, Analysis and control of products obtained from pyrolysis of polypropylene using a reflux semi-batch reactor and GC-MS/FID and FT-ICR MS, J. Anal. Appl. Pyrolysis 169 (2023), 105826, https://doi.org/10.1016/J.JAAP.2022.105826.
[28] J. Valecillos, I. Hita, E. Sastre, A.T. Aguayo, P. Castaño, Implications of Co-feeding water on the growth mechanisms of retained species on a SAPO-18 catalyst during the methanol-to-olefins reaction, ChemCatChem 13 (2021) 3140–3154, https://doi.org/10.1002/CCTC.202100124.
[29] I. Hita, H.O. Mohamed, Y. Attada, N. Zambrano, W. Zhang, A. Ramírez, P. Castaño, Direct analysis at temporal and molecular level of deactivating coke species formed on zeolite catalysts with diverse pore topologies, Catal. Sci. Technol. (2023), https://doi.org/10.1039/D2CY01850K.
[30] F. Aubriet, T. Ghislain, J. Hertzog, A. Sonnette, A. Dufour, G. Mauviel, V. Carré, Characterization of biomass and biochar by LDI-FTICRMS – Effect of the laser wavelength and biomass material, J. Am. Soc. Mass Spectrom. 29 (2018) 1951–1962, https://doi.org/10.1007/S13361-018-2005-Z.
[31] J. Hertzog, V. Carré, L. Jia, C.L. Mackay, L. Pinard, A. Dufour, O. Mašek, F. Aubriet, Catalytic fast pyrolysis of biomass over microporous and hierarchical zeolites: characterization of heavy products, ACS Sustain. Chem. Eng. 6 (2018) 4717–4728, https://doi.org/10.1021/ACSSUSCHEMENG.7B03837.
[32] F. Schmidt, C. Hoffmann, F. Giordanino, S. Bordiga, P. Simon, W. Carrillo-Cabrera, S. Kaskel, Coke location in microporous and hierarchical ZSM-5 and the impact on the MTH reaction, J. Catal. 307 (2013) 238–245, https://doi.org/10.1016/J.JCAT.2013.07.020.
[33] F. Aubriet, V. Carré, Fourier transform ion cyclotron resonance mass spectrometry and laser: a versatile tool, Fundam. Appl. Fourier Transform Mass Spectrom. (2019) 281–322, https://doi.org/10.1016/B978-0-12-814013-0.00010-7.
[34] J. Hertzog, V. Carré, F. Aubriet, Contribution of Fourier transform mass spectrometry to bio-oil study, Fundam. Appl. Fourier Transform Mass Spectrom. (2019) 679–733, https://doi.org/10.1016/B978-0-12-814013-0.00022-3.
[35] H. Wang, A. Gross, J. Liu, Influence of methanol addition on bio-oil thermal stability and corrosivity, Chem. Eng. J. 433 (2022), 133692, https://doi.org/10.1016/J.CEJ.2021.133692.
[36] L. Du, Z. Luo, K. Wang, F. Miao, Q. Qian, Catalytic co-conversion of poplar pyrolysis vapor and methanol for aromatics production via ex-situ configuration, J. Anal. Appl. Pyrolysis 165 (2022), 105571, https://doi.org/10.1016/J.JAAP.2022.105571.
[37] A.G. Gayubo, B. Valle, A.T. Aguayo, M. Olazar, J. Bilbao, Attenuation of catalyst deactivation by cofeeding methanol for enhancing the valorisation of crude bio-oil, Energy Fuels 23 (2009) 4129–4136, https://doi.org/10.1021/ef900301y.
[38] J. Haydary, P. Šuhaj, J. Husár, Waste biomass to methanol–optimisation of gasification agent to feed ratio, Biomass-.-. Convers. Biorefinery 11 (2021) 419–428, https://doi.org/10.1007/s13399-020-00692-3.
[39] A. Poluzzi, G. Guandalini, S. Guffanti, M. Martinelli, S. Moioli, P. Huttenhuis, G. Rexwinkel, J. Palonen, E. Martelli, G. Groppi, M.C. Romano, Flexible power and biomass-to-methanol plants with different gasification technologies, Front. Energy Res 9 (2022) https://www.frontiersin.org/articles/10.3389/fenrg.2021.795673.
[40] A.G. Gayubo, B. Valle, A.T. Aguayo, M. Olazar, J. Bilbao, Pyrolytic lignin removal for the valorization of biomass pyrolysis crude bio-oil by catalytic transformation, J. Chem. Technol. Biotechnol. 85 (2010) 132–144, https://doi.org/10.1002/jctb.2289.
[41] B. Valle, B. Aramburu, A. Remiro, A. Arandia, J. Bilbao, A.G. Gayubo, Optimal conditions of thermal treatment unit for the steam reforming of raw bio-oil in a continuous two-step reaction system, 2017. https://doi.org/10.3303/CET1757035.
[42] A.T. Aguayo, D. Mier, A.G. Gayubo, M. Gamero, J. Bilbao, Kinetics of methanol transformation into hydrocarbons on a HZSM-5 zeolite catalyst at high temperature (400-550 °c), Ind. Eng. Chem. Res. 49 (2010) 12371–12378, https://doi.org/10.1021/IE101047F.
[43] Q. Che, W. Yi, Y. Liu, X. Wang, H. Yang, H. Chen, Effect of mesopores in ZSM-5 on the catalytic conversion of acetic acid, furfural, and guaiacol, Energy Fuels 35 (2021) 6022–6029, https://doi.org/10.1021/ACS.ENERGYFUELS.0C04415.
[44] T.A. Palankoev, K.I. Dement'ev, D.V. Kuznetsova, R.S. Borisov, A.L. Maximov, S. N. Khadzhiev, Acetone reaction pathways as a model bio-oxygenate in a hydrocarbon medium on zeolite Y and ZSM-5 catalysts: Isotope labeling study, Chem. Eng. J. 431 (2022), 134228, https://doi.org/10.1016/J.CEJ.2021.134228.
[45] T.A. Palankoev, K.I. Dement'Ev, D.V. Kuznetsova, G.N. Bondarenko, A.L. Maximov, Acetone reaction pathways as a model bio-oxygenate in a hydrocarbon medium on zeolite y and ZSM-5 catalysts: in situ FTIR study, ACS Sustain. Chem. Eng. 8 (2020) 10892–10899, https://doi.org/10.1021/ACSSUSCHEMENG.0C03215.
[46] H. Zhang, C. Yang, Y. Tao, M. Chen, R. Xiao, Catalytic cracking of model compounds of bio-oil: Characteristics and mechanism research on guaiacol and acetic acid, Fuel Process. Technol. 238 (2022), 107512, https://doi.org/10.1016/J.FUPROC.2022.107512.
[47] Q. Bu, H. Lei, A.H. Zacher, L. Wang, S. Ren, J. Liang, Y. Wei, Y. Liu, J. Tang, Q. Zhang, R. Ruan, A review of catalytic hydrodeoxygenation of lignin-derived phenols from biomass pyrolysis, Bioresour. Technol. 124 (2012) 470–477, http://www.sciencedirect.com/science/article/pii/S0960852412012849.
[48] H. Kawamoto, H. Morisaki, S. Saka, Secondary decomposition of levoglucosan in pyrolytic production from cellulosic biomass, J. Anal. Appl. Pyrolysis 85 (2009) 247–251.
[49] G. Chen, R. Zhang, W. Ma, B. Liu, X. Li, B. Yan, Z. Cheng, T. Wang, Catalytic cracking of model compounds of bio-oil over HZSM-5 and the catalyst deactivation, Sci. Total Environ. 631–632 (2018) 1611–1622. ⟨http://www.sciencedirect.com/science/article/pii/S0048969718309070⟩.
[50] Á. Ibarra, I. Hita, M.J. Azkoiti, J.M. Arandes, J. Bilbao, Catalytic cracking of raw bio-oil under FCC unit conditions over different zeolite-based catalysts, J. Ind. Eng. Chem. 78 (2019) 372–382, https://doi.org/10.1016/j.jiec.2019.05.032.
[51] Z. Si, W. Lv, Z. Tian, K. Bi, X. Zhang, C. Wang, C. Pang, R. Dong, L. Ma, Conversion of bio-derived phenolic compounds into aromatic hydrocarbons by co-feeding methanol over γ-Al2O3, Fuel 233 (2018) 113–122, https://doi.org/10.1016/j.fuel.2018.06.031.
[52] L. Landa, A. Remiro, J. Valecillos, B. Valle, J. Bilbao, A.G. Gayubo, Unveiling the deactivation by coke of NiAl2O4 spinel derived catalysts in the bio-oil steam reforming: Role of individual oxygenates, Fuel 321 (2022), https://doi.org/10.1016/J.FUEL.2022.124009.
[53] O. Marie, A.V. Ignatchenko, M. Renz, Methyl ketones from carboxylic acids as valuable target molecules in the biorefinery, Catal. Today 367 (2021) 258–267, https://doi.org/10.1016/J.CATTOD.2020.03.042.

[54] R. Rebolledo-Leiva, M.T. Moreira, S. González-García, Offsetting the environmental impacts of single or multi-product biorefineries from wheat straw, Bioresour. Technol. 361 (2022), 127698, https://doi.org/10.1016/J.BIORTECH.2022.127698.

[55] Y. Zhou, V. Kumar, S. Harirchi, V.S. Vigneswaran, K. Rajendran, P. Sharma, Y. Wah Tong, P. Binod, R. Sindhu, S. Sarsaiya, D. Balakrishnan, M. Mofijur, Z. Zhang, M. J. Taherzadeh, M. Kumar Awasthi, Recovery of value-added products from biowaste: a review, Bioresour. Technol. 360 (2022), 127565, https://doi.org/10.1016/J.BIORTECH.2022.127565.

[56] B. Wang, G. Manos, A novel thermogravimetric method for coke precursor characterisation, J. Catal. 250 (2007) 121–127, https://doi.org/10.1016/J.JCAT.2007.05.018.

[57] J. Valecillos, J. Ruiz-Martinez, A.T. Aguayo, P. Castaño, Combined ex and in situ measurements elucidate the dynamics of retained species in ZSM-5 and SAPO-18 catalysts used in the methanol-to-olefins reaction, Chem. – A Eur. J. 27 (2021) 6719–6731, https://doi.org/10.1002/CHEM.202004865.

[58] P. Magnoux, H.S. Cerqueira, M. Guisnet, Evolution of coke composition during ageing under nitrogen, Appl. Catal. A Gen. 235 (2002) 93–99, https://doi.org/10.1016/S0926-860X(02)00242-9.

[59] T. Cordero-Lanzac, R. Palos, I. Hita, J.M. Arandes, J. Rodríguez-Mirasol, T. Cordero, J. Bilbao, P. Castaño, Revealing the pathways of catalyst deactivation by coke during the hydrodeoxygenation of raw bio-oil, Appl. Catal. B Environ. 239 (2018) 513–524, https://doi.org/10.1016/J.APCATB.2018.07.073.

[60] I. Hita, T. Cordero-Lanzac, G. Bonura, F. Frusteri, J. Bilbao, P. Castaño, Dynamics of carbon formation during the catalytic hydrodeoxygenation of raw bio-oil, Sustain. Energy Fuels. 4 (2020) 5503–5512, https://doi.org/10.1039/D0SE00501K.

[61] M. Ibáñez, B. Valle, J. Bilbao, A.G.G. Gayubo, P. Castaño, M. Ibañez, B. Valle, J. Bilbao, A.G.G. Gayubo, P. Castaño, Effect of operating conditions on the coke nature and HZSM-5 catalysts deactivation in the transformation of crude bio-oil into hydrocarbons, Catal. Today 195 (2012) 106–113, https://doi.org/10.1016/j.cattod.2012.04.030.

[62] S. Lee, M. Choi, Unveiling coke formation mechanism in MFI zeolites during methanol-to-hydrocarbons conversion, J. Catal. 375 (2019) 183–192, https://doi.org/10.1016/J.JCAT.2019.05.030.

[63] B. Valle, P. Castaño, M. Olazar, J. Bilbao, A.G. Gayubo, Deactivating species in the transformation of crude bio-oil with methanol into hydrocarbons on a HZSM-5 catalyst, J. Catal. 285 (2012), https://doi.org/10.1016/j.jcat.2011.10.004.

[64] Á. Ibarra, A. Veloso, J. Bilbao, J.M. Arandes, P. Castaño, Dual coke deactivation pathways during the catalytic cracking of raw bio-oil and vacuum gasoil in FCC conditions, Appl. Catal. B Environ. 182 (2016) 336–346, https://doi.org/10.1016/j.apcatb.2015.09.044.

[65] X. Hu, Z. Zhang, M. Gholizadeh, S. Zhang, C.H. Lam, Z. Xiong, Y. Wang, Coke formation during thermal treatment of bio-oil, Energy Fuels 34 (2020) 7863–7914, https://doi.org/10.1021/acs.energyfuels.0c01323.